Collège Doctoral du Languedoc-Roussillon

THÈSE

Pour obtenir le grade de

Docteur

Délivré par l'**Université de Montpellier**

Préparée au sein de l'école doctorale **I2S**
Et de l'unité de recherche **LIRMM**

Spécialité: **Informatique**

Présentée par **Anas Mustafa Kharboutly**

Identification of the Acquisition System in Medical Images by Noise Analysis

Soutenue le 13 septembre 2016 devant le jury composé de

M. Gouenou COATRIEUX	Professeur	Télécom Bretagne	E aminateur
M. Vincent CHARVILLAT	Professeur	IRIT, INP Toulouse	E aminateur
M. Alessandro Piva	Professeur	Université de Florence, Italie	Rapporteur
M. Khalifa DJEMAL	MCF HDR	Université d'Evry Val d'Essone	Rapporteur
M. William PUECH	Professeur	LIRMM, Université de Montpellier	Directeur de thèse
M. Gérard Subsol	CR CNRS	LIRMM, CNRS	Co-encadrant
M. Denis Hoa	Médecin	IMAIOS	Invité

Acknowledgments

When new days begin, try to smile gratefully.
When something seems difficult, be sure that you can do it anyway! Even if you feel tired, just keep going!
Try to be the best you can.. At all times, Dare to be!

Firstly, I would like to express my deepest appreciation to my supervisor Prof. **William PUECH**, head of ICAR (Image & Interaction) project, for the continuous support during my Ph.D studies, for his patience, and immense knowledge. His guidance helped me through my research. I could not have imagined having a better advisor and mentor for my Ph.D studies.
I owe a deep sense of gratitude to my co-supervisor Dr. **Gérard SUBSOL**. His prompt inspirations, timely suggestions, enthusiasm and dynamism have enabled me to complete my thesis.

My sincere thanks go to my PhD reviewers Prof. **Alessandro PIVA** and Dr. **Khalifa DJEMAL**, who accepted to read and evaluate my research work. Your remarks and suggestions have helped me to improve the quality of my manuscript.

My sincere thanks also go to: Prof. **Gouenou COATRIEUX** and Prof. **Vincent CHARVILLAT**, for being a part of the jury of my Ph.D thesis.

I would like to extend my sincere thanks to my lab-mates, my work family: **ICAR Team**. For all the splendid moments we spent together in the different activities in and out of the work context.

A special thanks for **IMAIOS** company, especially Dr. **Denis HOA**, for all the acquisitions they provided us during our different research steps.

My deepest thanks to my **new family in France**: my friends, for being a part of each moment in my new life here.
My deepest thanks also to **my friends outside France**, for their unlimited support.

The largest thanks and appreciation to **my parents**, **my brothers and my sister**, for supporting me spiritually all the time.

Last but not the least, I would like to thank my motherland: **Syria**, with the hope that the war ends soon.

And to the country who welcomed me and provided me a high quality of research environment to continue my achievements: **France**.

Identification of the Acquisition System in Medical Images by Noise Analysis

Abstract: Medical image processing aims to help the doctors to improve the diagnosis process. Computed Tomography (CT) Scanner is a medical imaging device used to create cross-sectional 3D images of any part of the human body. Today, it is very important to secure medical images during their transmission, storage, visualization and sharing among several doctors. For example, in image forensics, a current problem consists of being able to identify an acquisition system from only digital images. In this thesis, we present one of the first analysis of CT-Scanner identification problem. Our work is based on the camera identification methods to propose a solution for such kind of problem. It is based on extracting a sensor noise fingerprint of the CT-Scanner device. The objective then is to detect its presence in any new tested image. To extract the noise, we used a wavelet-based Wiener denoising filter. Then, we depend on the properties of medical images to propose advanced solutions for CT-Scanner identification. These solutions are based on new conceptions in the medical device fingerprint that are the three dimension fingerprint and the three layer one. To validate our work, we applied our experiments on multiple real data images of different CT-Scanner devices. Finally, our methods proved to be robust beside giving high identification accuracy. We were able to identify the acquisition CT-Scanner device as well as the acquisition axis.

Keywords: Medical image forensics, device identification, sensor noise, denoise filtering, device fingerprint.


FORENSICS
A closer look

Contents

List of Figures

List of Tables

Chapter 1

Introduction

Contents

1.1 Medical Imaging overview

Late in the twentieth century, medical imaging becomes the cornerstone in the world of medicine [Doi 2006]. It represents the tools that are used to have an internal vision of any anatomical part of the human body. When we talk about medical imaging, that does not mean the process of taking a photo and saving it as a memory on a hard disk only. Indeed, medical imaging helps medical doctors to improve and speed up the diagnosis process as well. Medical image processing refers to the applied technologies of image processing in medical disciplines [McAuliffe 2001]. In this regard, different devices and multiple modalities could be found [Beutel 2000].

Computed Tomography (CT) is an important modality used in medical imaging. It was first presented by G. N. Hounsfield in 1970, who was awarded with A. M. Cormack the Nobel Prize in medicine for the innovation of Computed Tomography. It is based on the computerized combination of two-dimensional cross-sectional x-ray images to produce a three dimensional image of an internal structure for any part of the human body. However, this imaging revolution required a development in the level of storage and transfer solutions [Seeram 2015].

DICOM (Digital Imaging and Communications in Medicine) is a standard image format for storing and transmitting medical images [Graham 2005]. In addition to image content, DICOM contains a header file that includes all the information about the patient and the acquisition system. Moreover, it contains some communication and networking protocols that ensure the easy transmission of these medical images among different users [Pianykh 2012].

1.2 Problem and work motivation

Security is one of the most important aspect to consider when we talk about data or image transmission [Pan 2010]. Although it becomes nowadays too easy to transmit or share the DICOM files [Bidgood 1997], it is critical to authenticate their content. DICOM files can be modified easily. So, different scenarios can be discussed when we think about securing medical images:

1. Health assurance: let us propose that someone wants to go to an assurance company to order a health assurance. The assurance company will ask him about his medical profile. This profile contains all the informations about his health situation, medical history and even his medical images. In such situation, two options could be considered. First, the client is healthy, so he will pay the normal fees for the assurance company. Second, the client has a health problem, so he has to pay additional fees to the assurance company because the probability of having a surgery is high. In the second case, the patient can take an another image of a healthy person, then he can edit its DICOM header to insert his personal informations with the device model. So, he removes all the informations about the disease, and can avoid the additional fees. However, if we are able to identify the CT-Scanner device from the image, we can go back to the source device dataset and retrieve the original image information.

2. Bank credits: let us suppose another one that wants to go to a bank and order credits for the next ten or twenty years in order to buy a new house or a new car. The bank will ask for his medical profile. Again, two options should be considered. First, the client is healthy, so the bank will accept his request and approve the required credits. Second, the client has a health problem, so the bank will refuse his request and

will not give him credits even for five years, because the probability of refunding his credits is less than usual. In this case, the patient can fake his own health informations by replacing it with this of someone healthy. So, his disease informations does not exist anymore, which encourage the bank to accept his request. Also, if we are able to identify the source CT-Scanner, we can avoid such kind of fraud.

3. In some cases, it is easier to convert the DICOM image into another format and share it, or even to make just a print screen of the image and send it by email. In this case, any header information will be lost. So, when the radiologist or the responsible person receives this image, identifying the source CT-Scanner device becomes the only way to retrieve the required informations.

4. In the industry side, when the industrial CT-Scanner produces an image, the enterprise may convert it to another format for sharing purposes. This conversion will produce images without any header file. In this case, It is also important to identify the CT-Scanner, then to retrieve the original image informations. So, we can conserve the copyrights and avoid image attacking in the absence of the header file, since we can authenticate the transmitted image.

1.3 Contributions

The main objective of our work is to identify the CT-Scanner device from its images especially for authentication purpose. This is exactly the objective of what is called image forensics [Fridrich 2009]. Image forensics addresses two essential problems: device identification [Liu 2010] and forgery tracing [Farid 2009, Yerushalmy 2011]. Our work consists of identifying the CT-Scanner from its output images by noise analysis. In this analysis, we

present four contributions to achieve the required goal. We based on digital camera identification methods to propose our solutions, and the key point of our contributions is to extract the CT-Scanner sensor noise from its images:

1. We assume that the CT-Scanner acquisition sensor leaves noise as a fingerprint in each acquired image. The proposed method consists of two parts. First, extracting the Reference Pattern Noise (RPN) from a given CT-Scanner as its fingerprint. Second, detecting its presence in any new tested image by correlation. The extracted noise in this proposed method was not pure, since it contains some traces of the content scene [Kharboutly 2014].

2. We provide some improvements on the previous proposition in order to avoid the scene traces. We eliminate these traces in the noise image by a binary generated mask. Then, we present a new RPN and a correlation map concept. This correlation map gives more importance to the unmasked parts of the processed images than the other ones. Finally, the correlation is computed with respect to the correlation map [Kharboutly 2015b].

3. Based on the previous method and the specificity of 3D medical images, we produce a new CT-Scanner fingerprint which is composed of one RPN for each axis. The objective is to identify a tested slice even if the original image was attacked by rotation [Kharboutly 2015a].

4. Based on the first contribution and the intensity Hounsfield scaling in CT-Scanner image, we present a new CT-Scanner fingerprint, which consists of three layer RPNs. We apply our work on each layer separately. Finally, we are able to identify the source CT-Scanner of a real tested slice when two of its layers correspond to the same CT-Scanner device.

1.4 Thesis organization

The goal of this thesis is to give a documentation about our contributions. We aim to give a complete research on the medical image forensics, in particular, the CT-Scanner identification. This thesis is organized in four main chapters as follows:

- Chapter 2 provides an overview of the CT-Scanner, its acquisition chain and how it works. The DICOM format and our work orientation are also presented in this chapter.
- Chapter 3 studies different researches presented in the literature about device identification either in the photography application or in the medical one.
- Chapter 4 explains our first group of contributions that are based on the digital camera identification.
- Chapter 5 presents our second group of contributions that are based on the specificity of medical images.

In chapter 6 we conclude this thesis by some discussions and present our vision for a future work in this domain. In Chapter 7 a summary of our work is given in French.

Chapter 2

Introduction to CT-Scanner imaging

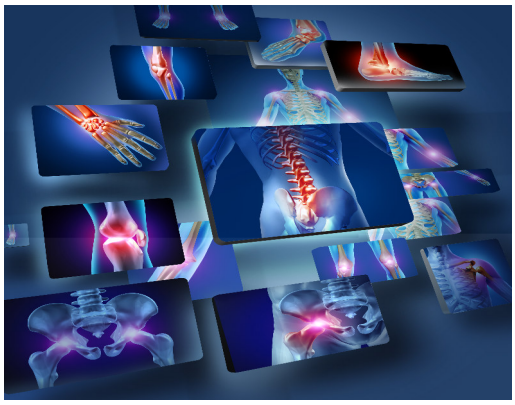

Contents

2.1 Introduction

Medical imaging is the application of digital imaging for medical objectives. It is considered as an important part in the world of medicine. It refers to the different interactions between some forms of energy, which penetrate the tissues in order to have an internal view of any part of the human body without need to be opened up surgically [Bushberg 2011]. It is used to help the doctors in examination and diagnosis process by giving a quite good image quality. Most medical imaging systems require the interaction between this energy and the tissue where it goes throw. Without any kind of interaction like absorption or attenuation for example, the detectors of this energy will not be able to extract any useful information about the imaged tissues, consequently no image will be acquired using such information [Wolbarst 2013]. Different modes of medical imaging are existed regarding the different types of energy which used in the image acquisition. These modes are called the modalities [Leondes 2005]. These modalities include:

- Radiography: The first generation technology of medical imaging [Sutton 1987]. It is composed of an X-ray sender in front of the patient and an X-ray receiver on the other side. A pack of x-ray is sent by the x-ray tube through the patient tissues. These x-rays interact with the patient tissues, and some of it reach the detector. This process constructs the radiographic image [Benseler 2006]. Fig. 2.1 illustrates an example of a radiography imaging device, and images for multiple anatomical parts of the human body.

- Magnetic Resonance Imaging: An imaging technology that uses magnetic fields and radio waves to provide a detailed images of the soft tissues [Edelman 1993]. It is used for disease detection and diagnosis purposes. By using protons that are so sensitive to magnetic fields, it

Figure 2.1: Radiography image

can produce the MRI images. Protons are centered in each hydrogen atom of water molecules of the human body. During the acquisition, bursts of radio waves are sent through a specific anatomical part of the patient. These waves change the alignment of exited protons in this anatomical part. Then, when the radio waves are stopped, the affected protons are realigned. These affected protons, in their turn, send radio signals to be collected by the receivers. These signals contain information about the exact location of imaged protons. Finally, the combination of millions of protons signals creates a detailed images of the anatomical part. MRI scans the anatomical part along a directional axis. The generated slices are 2D, where it divides the anatomical part in a series of 2D slices. Then, these generated slices are combined together to give the 3D MRI image [Kuperman 2000]. Fig. 2.2 illustrates an example of an MRI imaging device and an MRI image of a brain.

- Ultrasound Imaging: One of the most used imaging technology. That is portable and radiation free [Von Ramm 1990]. It provides also a cross-sectional view of the imaged anatomical part of the human body. Moreover, it can be acquired in real time, that makes it a good indicator for

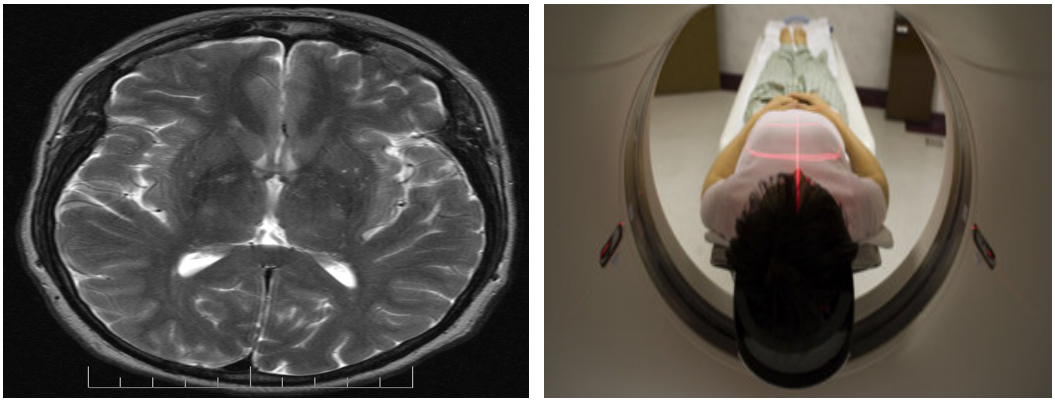

Figure 2.2: MRI image

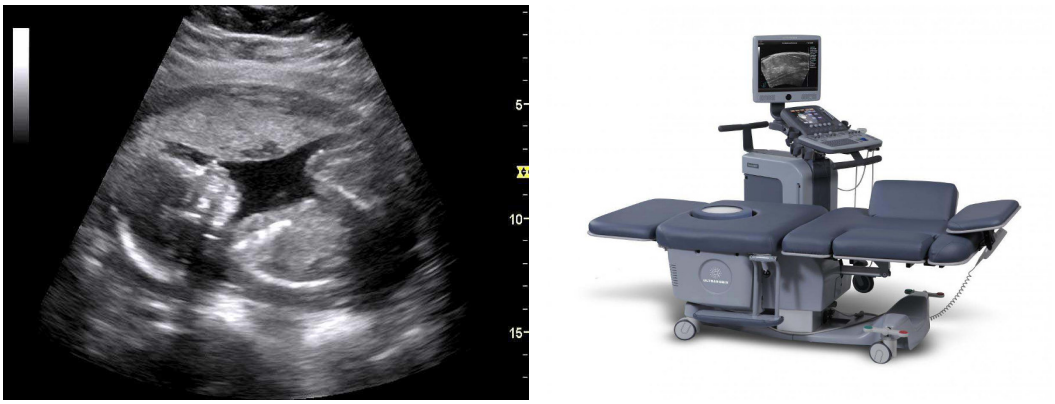

Figure 2.3: Ultrasound image

the interventions. The ultrasound signals pass through the tissues, some of it are reflected back to the transducer (echo signals). The echo signals are used to construct the ultrasound image. The ultrasound transducer works as a sender and a receiver as well [Del Cura 2012]. Fig. 2.3 illustrates an example of an ultrasound imaging device, and an ultrasound image of a fetus.

- Nuclear medicine: Produces detailed images of what is happening in the human body at the cellular level. It is used to study the body function,

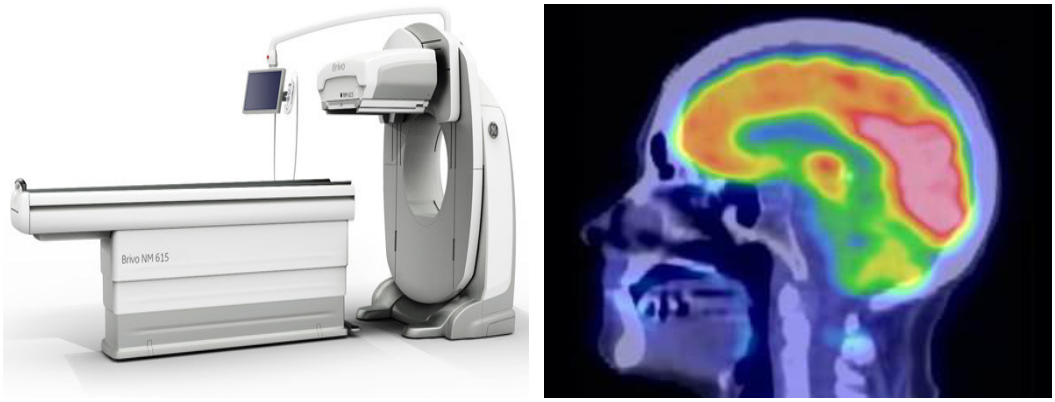

Figure 2.4: Nuclear medicine image

measure its chemical and biological processes [Mettler Jr 2011]. During the acquisition, radio-tracers are injected into the bloodstream of the human body. These radio-tracers go through the anatomical part and send out energy in a form of gamma rays. Then, special imaging sensors detect the gamma rays and send it to the computer in order to create the image. This imaging system provides special information that cannot be acquired using other imaging system [Cherry 2012]. Fig. 2.4 illustrates an example of Nuclear medicine imaging device and an image of a head.

- Computed Tomography: Computed Tomography or what is called CT-Scanner imaging, is an imaging technology, which integrates a series of x-rays views that are captured from so many different angles to create cross-sectional images [Lisle 2012]. It provides a 3D representation for any part of the body. By passing this body part through a circular tube which contains an x-rays sender and a set of detectors on the opposite side, these detectors collect the acquisition object information and send it to a computer which processes it, then displays it as a gray-scale image to the user. It is widely used since it provides a lot of information about the patient, physical features and potential disease [Hsieh 2009].

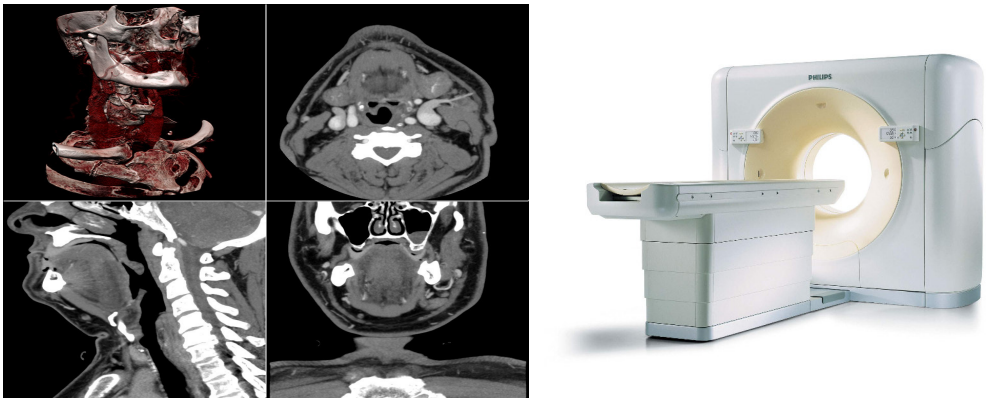

Figure 2.5: CT-Scanner image

Fig. 2.5 illustrates an example of a CT-Scanner device and an image of a neck.

CT-Scanner is one of the most used imaging system in the medical imaging world [Brown 2008]. The image of the anatomical part of the human body could be reconstructed based on a large number of projections. Fig. 2.6 illustrates this process. The energy is sent from the source, then, passed though tissues, and finally, projected onto detectors, which in their turn sent it to the computer for post-processing and constructing a clear internal image of the anatomical part.

2.2 CT acquisition chain

The CT-Scanner imaging system is composed of three basic parts: data acquisition, image reconstruction and image display [Seeram 2015], as illustrated in Fig. 2.7

- Data Acquisition: It represents the process of x-rays which are sent from the source x-ray tube, passed through the patient and received by the detectors. When the x-rays passed through the patient and reached the

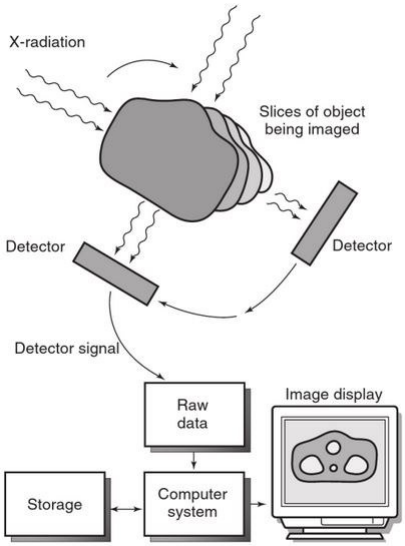

Figure 2.6: Image acquisition and reconstruction [Seeram 2015]

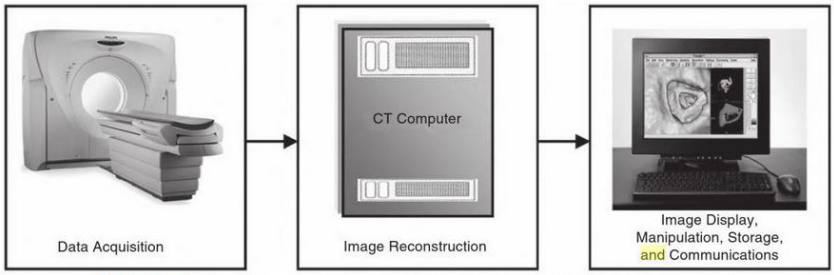

Figure 2.7: CT-Scanner imaging system [Seeram 2015]

detector, it registers the received information values. This information includes the transmission and attenuation values. Then, rotating the x-rays tube and these detectors several times during the patient movement will produce a 3D image rather than just a 2D slice only, since one slice is generated per each rotation [Ketcham 2001]. At the end of this step, enough information should be registered in order to continue the reconstruction step. However, many parameters should be tuned during the acquisition step, these parameters include: **Beam Energy**: (80-140)

Kv, which corresponds to the energy of x-rays beam that is sent from the x-rays tube. Increasing beam energy will speed up the electrons, and produce more energy. **Tube current**: (20-500) mA, it represents the x-rays beam intensity, or the quantity of the sent electrons. **Scan time**: (0.3-4) s, is the x-rays production time in one rotation. Increasing this time will increase x-rays quantity. **Slice thickness**: (0.5-10) mm, thickness along 'Z' axis. **Pitch**: (0.5-2) s, is the table movement speed in one rotation. Moreover, the data acquisition step includes two conversion cycles. The first one is when detectors receive the x-rays and convert them into electrical signals using the electrical detectors. The second one, represents the conversion of electrical signals into digital values that will be used later in the reconstruction step.

- Image Reconstruction: The collected information from detectors is sent to a computer for the 3D reconstruction [Hsieh 2006]. The computer uses mathematical techniques for the tomography reconstruction in order to reconstruct 3D images. These 3D images are reconstructed from a series of cross-sectional planes that are acquired along 'Z' axis. These techniques are called the reconstruction algorithms. Several reconstruction algorithms are existed like filtered back-projection, which is commonly used in the iterative reconstruction algorithms that are widely used in the modern generation of CT-Scanners [Hsieh 2013, Beister 2012, Cierniak 2011]. Although the principles of these algorithms are known, their implementations are not described by the manufacturers. Many parameters should be tuned during the reconstruction step, these parameters include: **FOV**: (10-50) cm, is the reconstruction field of view, which represents the image size in 'X' and 'Y' directions [Hsieh 2004]. **Reconstruction matrix**: (512×512), is the image resolution. **Convolution kernel/Reconstruction filter**:

includes the bone filter for hard details and soft tissue filter for smoothed details.

- Image Display: The reconstructed image is then stored to be viewed or analyzed later using known softwares.

The first CT-Scanner was presented in 1972 by Sir Godfrey Hounsfield [Jones 2013]. Earlier CT-Scanners had acquired images of one slice at a time. In the next generations that allows an x-rays tube to go around the patient were known as helical or spiral CT to acquire images of multiple slices, one slice for each tube rotation. This generation gives the ability of imaging larger anatomical parts of the human body. Recent generations of CT-Scanners have proposed the multiple rows of detectors, where the images of multiple slices can be acquired, where multiple slices are acquired by a tube rotation. This generation provides a larger area of the patient to be imaged as illustrated in Fig. 2.8.

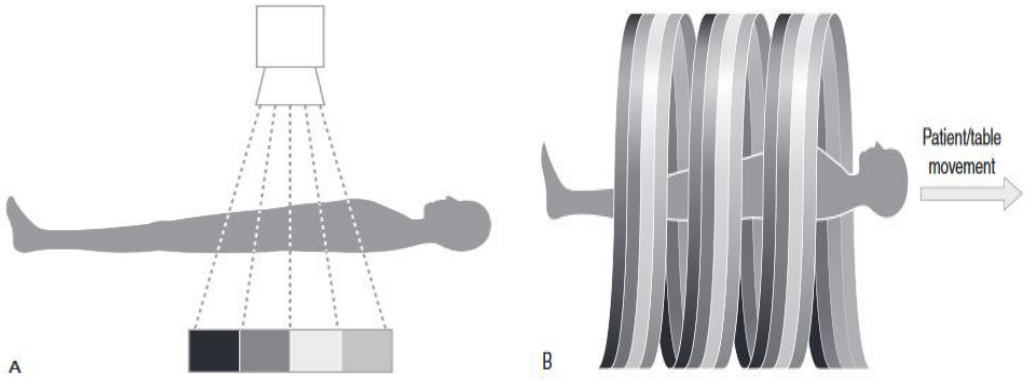

Figure 2.8: (A)Multi-detector system. (B) Multi-slice CT [Seeram 2015].

2.3 How the CT-Scanner works

The patient is positioned on the CT-Scanner table. The source sends x-rays through the anatomical part of the body to be imaged. The detector on the other side of the patient receives these x-rays and registers their received or attenuated values. Both x-rays source and detectors are located inside the CT-Scanner gantry and rotated around the patient during acquisition [Bushberg 2011]. CT-Scanner detectors convert x-rays photons into digital values to be sent to the computer. CT-Scanner has an indirect detector. It consists of two parts: a scintillator and a silicon photodiode. The scintillator is the first part that collects x-rays that are sent from the source and passed through the patient. The scintillator then converts the received x-rays photons to light. The silicon photo-diode then collects this light and converts it into an electrical current. Finally, the electrical current is passed to an analogue-to-digital converter [Kagadis 2011]. However, this acquisition system produces two types of noise. First, a quantum multiplicative noise that is resulted from a random number of photons sent by the x-ray tube and the inhomogeneity of silicone material of the photo-diode. Second, an electrical additive noise that is added to the image signal during the analogue-to-digital converter. After computer receives the digital acquisition values, it applies the reconstruction step using an appropriate algorithm to reconstruct the final image. Although all the CT-Scanners use similar reconstruction algorithms, but all of their information and parameters are not accessible. Each CT-Scanner slice is divided into voxels. The dimensions of the CT-Scanner slice may reach to to 1024 x 1024 voxels. During the reconstruction process, specific attenuation values are allocated to each voxel. The final reconstructed image in then formed as a two dimensional array of pixels. The pixel value of the reconstructed image is calculated as an average of all attenuation values of the same volume voxel. This value is compared to the attenuation value of water

and displayed in a scale of Hounsfield Unites (HU). In the HU, water takes an attenuation value of zero. The range of HU is 2000 and may reach in some CT-Scanners to 4000 located in the gray level. Where (-1000) value represents the intensity of air and (+1000 or +3000) value represents the intensity of compact bone. Fig. 2.9 illustrates the range of CT-Scanner values regarding Hounsfield scale [Hounsfield 1980]. Fig. 2.10 illustrates an example of a slice

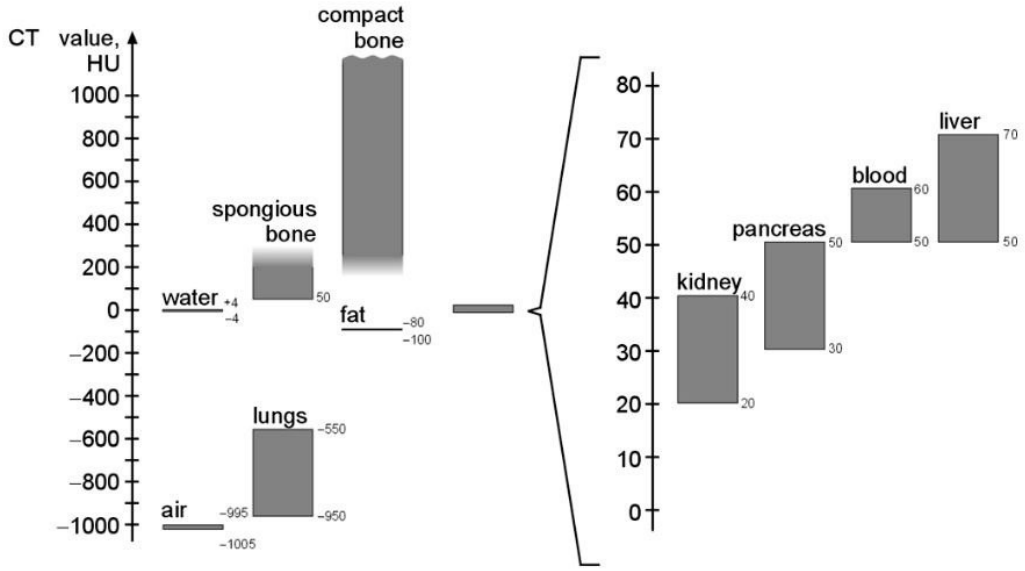

Figure 2.9: Range of Hounsfield scale.

from a 3D image of crane, and its different values regarding Hounsfield scale.

Finally the image is stored to be viewed later or adjusted for diagnosis purposes.

2.4 DICOM Format

Medical images are usually stored in an international standard of Digital Imaging and Communications in Medicine (DICOM). DICOM files consist of two

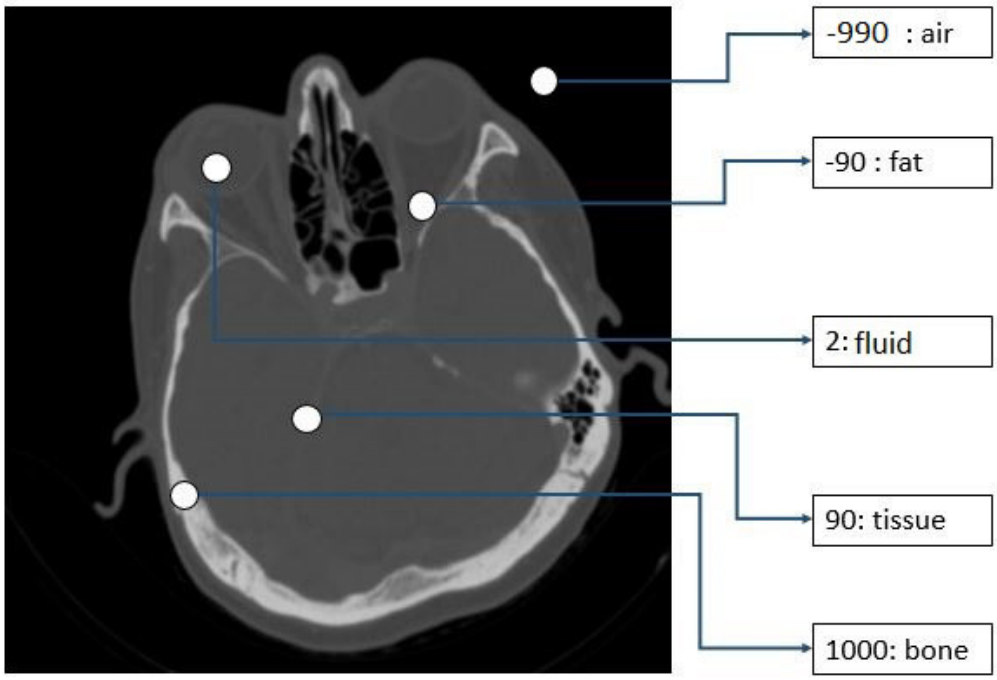

Figure 2.10: Slice from 3D image of crane.

parts, a header and an image content [Toennies 2012]. The header contains a mandatory set of data elements the contain information about the medical image. These informations include (patient information, acquisition parameters, acquisition data and acquisition device...etc). While the second part represents the medical image content.

2.5 Problematical orientation

In case of absence or unauthenticated meta-data about DICOM file, we are in critical situation since the medical image content can not be authenticated. So, we need to authenticate the medical image based on the image content only. Our aim is to identify the source CT-Scanner as a blind device identification using the image content only. Then by comparing with the meta-data

information we can decide whether to authenticate the medical information content or not. Based on the image content we will extract the noise in order to analyze it later and identify the source CT-Scanner of any tested CT-Scanner image.

Chapter 3

Digital Device Identification

Contents

3.1 Introduction

Image forensics is the applied technology that concerns about retrieving an evidence about the source acquisition device [Redi 2011]. It is an important field of research that aims to authenticate images by retrieving information about their history in case of unauthenticated source information or content modification. Two basic branches exist when we talk about digital image forensics [Piva 2013, Farid 2008]. The first one represents the group of methods which aims to identify the device that acquires the image [Jenkins 2009], or to decide whether a specific device is the source of this image or not [Sencar 2013]. These methods depend on analyzing the image content to detect an evidence of the source device, and are called source device identification tools [Geradts 2002]. The second group represents the methods that study the original image statistics in order to trace the image forgery. This group of methods is called tampering detection tools [Mahdian 2010]. Digital camera identification is the application of first group methods. It is used to authenticate the source device information. Many works have been done in this area to achieve this goal [Lukas 2006, Chen 2008, Chen 2007b]. On the other hand, device identification is not limited to the digital camera, but also to the medical devices. Medical device identification is the used methods for retrieving information about the source medical device in case of absence or unauthenticated acquisition information [Chen 2007a]. In more particular, CT-Scanner identification aims to authenticate the CT-Scanner in case of absence or unauthenticated DICOM information. The rest of this chapter is organized as follows. In Section 3.2 we present an analysis of the sensor noise and its application for digital device identification. In Section 3.3 we present the identification of the acquisition device in the medical domain. In Section 3.4 we provide our conclusion.

3.2 Noise analysis

One of the most popular techniques used for digital device identification is Sensor Pattern Noise (SPN). SPN is used for digital camera identification. It analyses the sensor output in order to identify the source camera. Since it is not possible to access to the camera sensor output, the idea is to characterize the noise in the camera image output. But before going into the digital camera identification, we are in need to know the different patterns that constitute the SPN. In Section 3.2.1 we present the different patterns that constitute the SPN. In Section 3.2.2 we present the usage of SPN for camera identification purpose. In Section 3.2.3 we provide some improvements on the camera identification methods based on the SPN. In Section 3.2.4 we give some applications of SPN for digital device identification.

3.2.1 Sensor Pattern Noise

In fact, there are two basic components of the SPN as illustrated in Fig. 3.1. They are the Fixed Pattern Noise (FPN) and the Photo-Response Non-Uniformity (PRNU) [Lukas 2006]. FPN represents the pixel to pixel differ-

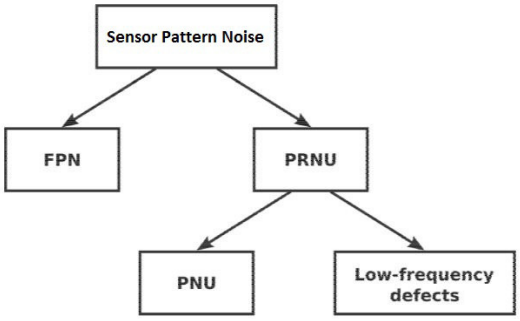

Figure 3.1: Sensor Pattern Noise

ence [Mohammadnejad 2011], it is caused by dark currents when the sensor is not exposed to light. It is about an additive noise and is removed from the

output image by subtracting an empty dark frame from each acquired image. Since FPN is not stable under temperature nor time, it cannot characterize the sensor noise. On the other side, the PRNU forms the main part of SPN. It is basically caused by the Pixel Non-Uniformity (PNU) in addition to some low frequency components. Low frequency components are caused by light refraction, it cannot characterize the sensor noise because it is not related to the camera sensor. PNU is caused by different sensitivity of pixels to light regarding the inhomogeneity of silicon wafers and imperfections during the sensor manufacturing [Lukas 2006]. So, it is a unique pattern regarding each camera sensor, and it can be used for identification purposes.

3.2.2 PRNU-based identification methods

PRNU has many properties that make it an optimal solution for the problem of digital camera identification [Costa 2012, Goljan 2008b]. These properties are:

- Stability: It is stable over time and under different physical operations.
- Generality: Each camera sensor has a unique pattern noise.
- Universality: Each image of the same camera inherits it.
- Dimensionality: It has a larger information content of camera sensor.
- Robustness: It is robust against different processing operators.

A lot of work has been done on the digital camera identification based on the PRNU. It was first proposed by [Lukas 2006]. Their method aims to extract the PRNU pattern from a camera output, then to detect its presence in any new image of this camera. This detection was applied by correlation like watermark detection method [Cox 2002]. Their method is composed of two parts. The first part consists of extracting the camera Reference Pattern Noise

(RPN) that characterizes the PRNU sensor noise. The second part consists of detecting the presence of this RPN in any test image by correlation. To extract the RPN of a camera, two basic steps are included. The first step is to select a group of images of this camera and extract their noise component, because this noise component or noise residual, in other words, can characterize the PRNU noise. The second one is to average the noise components to build one image that represents the RPN of the studied camera sensor. This RPN represents an approximation of the PRNU of the studied camera. It is a unique noise pattern for a given digital camera and can be served as a unique fingerprint that can be used for identification purposes:

$$RPN = \frac{1}{N}\sum_{i=1}^{N} W_i, \tag{3.1}$$

where W_i is the noise component of the i^{th} image and N is the number of images. To decide whether an image was acquired by a specific camera or not, the correlation between the noise component of this image and the RPN of the specific camera is computed. If the correlation value is larger than a specific threshold, then the source camera of this image is identified. In other cases, any other correlation between the noise component of this image and any other RPN of another camera should have a value smaller than this correlation value. Fig. 3.2 illustrates the general schema of digital camera identification. To extract the noise component of an image, the authors based on [Mihcak 1999] to apply a wavelet decomposition and use Wiener denoising filter:

$$X_{den}(i,j) = X(i,j)\frac{\hat{\sigma}^2(i,j)}{\hat{\sigma}^2(i,j) + \sigma_0^2}, \tag{3.2}$$

where X is the wavelet sub-band. And finally, they subtracted the denoised image from the original one to keep the noise component only. Since they focused only on the PNU component of the RPNU, the noise extraction was applied to ignore any other low frequency noise components, so we can consider the PNU as the extracted PRNU pattern noise. An average phase was

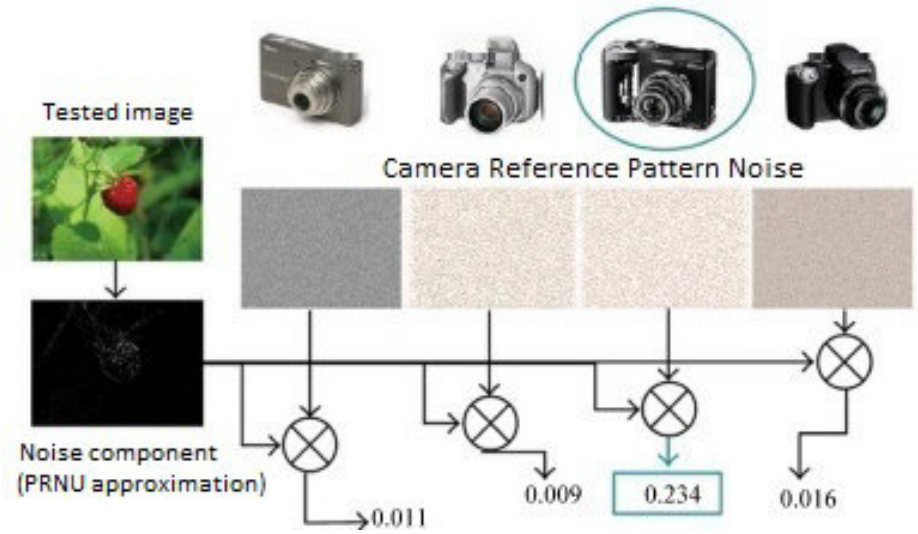

Figure 3.2: Digital camera identification [Piva 2013]

applied to remove any additive noise caused by FPN. In fact, this RPN has two problems. First, it contains some noise artifacts in addition to sensor noise. Second, it is affected by JPEG compression as visual patterns. Fig. 3.3 illustrates the noise artifacts. Where (a) is the acquired image by camera (d),

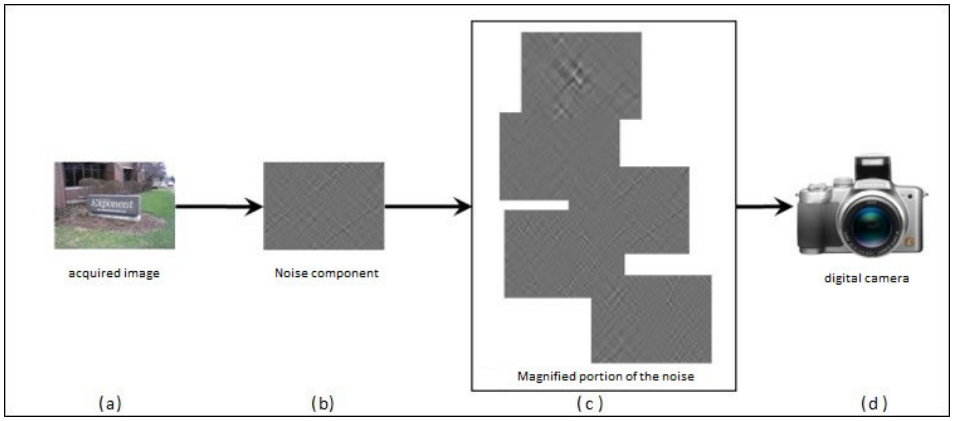

Figure 3.3: Noise artifacts.

(b) its noise component and (c) is the magnified noise artifacts.

Chen *et al.* present an improvement on the source camera identification depending on the estimation and detection of PRNU in digital images [Chen 2007a]. Their improvements were divided into three steps. First, they used the linear model of digital camera output and estimated the PRNU from noise residuals. They divided the RPN and a test image into blocks. Then, they used a normalized correlation as an optimal detector over all blocks to measure the similarity between a test image and an RPN. Second, they used the Neyman-Pearson test and estimated the probability of false rejection to specify a threshold value of the normalized correlation value regarding the studied camera to decide whether this is the source camera or not. Finally, they developed the RPN extraction to avoid the RPN noise artifacts. These periodic artifacts are caused by color interpolation. In fact, this kind of noise is not unique for one camera, so they applied a zero-mean operation to decrease these artifact effects. To avoid JPEG compression artifacts, they moved to the frequency domain by Fourier transformation. Then, they denoised Fourier magnitude by Wiener filter, so any additional artifacts caused by JPEG compression should be removed. Therefor, false alarms are decreased. Chen *et al.* extend their previous work to include the case of RPN attack problem by image modification [Chen 2007b]. They proposed two steps to achieve this goal. First, they estimated the RPN from non modified images. Second, they used a sliding window in both the RPN and an image noise component. Then, they computed the correlation and compared it with a threshold to decide whether this center pixel is modified or not. Chen *et al.* include their previous research tasks from [Chen 2007b] and [Chen 2007a] in one framework [Chen 2008]. Its goal is to identify the digital source camera and to verify the image integrity. Based on the PRNU, two tasks were achieved by RPN preprocessing: camera identification and forgery detection. They proposed the RPN as a unique fingerprint inserted into images by the camera sensor. They used the camera

sensor output to estimate the camera RPN:

$$RPN = \frac{\sum_{i=1}^{N} W_i I_i}{\sum_{i=1}^{N} I_i^2}, \tag{3.3}$$

where W_i is the noise component, I_i is the original image and N is the number of used images. Then, they applied some preprocessing corrections in order to remove any artifacts from the RPN caused by image acquisition steps. Then, they detected its presence in image blocks by the normalized correlation in order to both, identify the source camera of each block and verify its integrity. Based on binary hypothesis of Neyman-Pearson criterion they defined a threshold value to identify the source camera of each block and decide whether each block was modified or not. Finally, they evaluated their method robustness on different image processing operators and geometrical transformations. Their proposed framework decreased the error rate compared to [Lukas 2006].

Filler *et al.* used the RPN in order to identify both a digital camera brand and its model [Filler 2008]. They used a Support Vector Machine (SVM) in order to classify images regarding their source camera model and brand. For each studied camera model and brand, they selected a group of images to build an RPN regarding each camera model and brand. In addition to the sensor noise information in an RPN, there exists some traces or periodic patterns. These patterns are the result of the camera acquisition pipeline. The authors proposed that these patterns are different from one camera brand to another. So, they based on these patterns to identify the camera brand in addition to the RPN information that is used to identify the camera model. They proposed to quantify these patterns and use its features as an input of the SVM classifier. Finally, based on their experiments, they were able to classify the tested images according to the camera model and brand.

Goljan *et al.* extend their previous work in [Lukas 2006] on digital camera identification based on the RPN [Goljan 2008b]. Their proposed method was

able to identify the digital camera even if the tested image was processed. Two processing operators were studied, the case of cropping or scaling image and the case of applying digital zoom. They experimentally presented that they are able to retrieve both the scaling factor and cropping parameters.

Goljan *et al.* tested their previous method of camera identification based on a large amount of images in order to evaluate it [Goljan 2009]. They estimated the RPN of each studied camera using the previous method. Then, they detect its presence in an image by the Peak to Correlation Energy (PCE), that is used to measure the similarity by measuring the height of correlation peak. It is more stable than the normalized correlation since it is not related to the image size and depends only on the image content. Their experimental results show two important facts. Firstly, the non-unique patterns which exist in the RPN are related to the image content and they are the reason of increasing the error rate. So, it should be removed in order to keep the error rate at the same level. Secondly, the quality of used images in RPN building is a basic reason for false alarm.

3.2.3 Improved and advanced PRNU identification methods

Some improvements were proposed on PRNU method to increase the identification accuracy. Kang *et al.* presented a new RPN extraction method to enhance the camera identification performance [Kang 2012]. To achieve that, they removed the contamination of RPN artifacts caused by image content, JPEG compression and artifacts caused by processing operators during the image acquisition. They converted the noise component to the frequency domain by Discrete Fourier Transformation (DFT). Then, they extracted the RPN using the traditional method of [Cox 2002] but in the frequency domain. They applied an average operator on the real part of the Inverse DFT

to extract the RPN as follows:

$$RPN = real\left(IDFT\left(\frac{\sum_{i=1}^{N} W_i}{N}\right)\right), \tag{3.4}$$

where W_i represents the phase-only component and N is the number of images. Then, to detect its presence in any new image they proposed to use the Circular Correlation Norm (CCN) as a detector. CCN can lower the error rate to a half what is registered by PCE. It is better than both of PCE and normalized correlation. They experimentally presented that their identification method achieved a better performance since it is resistant to JPEG compression and not affected by image content or artifacts that appear during the different process steps.

Li proposed an improvement in [Li 2010], by demonstrating that the extracted RPN from an image contains additional artifacts caused by image content details and other periodic patterns. This caused an untrusted signal that is involved to the RPN due to the fact that any other artifacts increase the error rate. To solve this problem, Li proposed five models to reduce the effect of image content details. These models are based on user-managed thresholds. The basic objective of these models is to specify a weighting factor for the RPN components, where the smaller important components of RPN are given a high weighting factor, while the artifacts of image content are given a lower weighting factor. So, in the spatial domain, the extracted noise residual of RPN is preprocessed by each model in order to eliminate the effect of image content. Finally, the normalized correlation is used in order to detect the presence of RPN in any new test image. However, as the work is done in the spatial domain, important components of RPN may also be eliminated.

Other enhancements on PRNU methods were proposed in order to improve the identification performance. Shi *et al.* presented a neural network based method to decrease the image content [Shi 2014]. Their method based on the previous maximum likelihood estimator to estimate the RPN. Then, they

used the normalized correlation to measure the similarity between a tested image and the RPN of any digital camera. They used a neural network to estimate the weighting factor of image blocks. For each image which is used in the training or testing steps, a decomposition step is applied to divide the used image into blocks. Then, from each block they extracted two features, that are the intensity and the texture features:

$$f^{j}_{int,I_i} = \frac{1}{N_b} \sum_{(x,y)\in j_{th}block} I_i(x,y), \tag{3.5}$$

$$f^{j}_{text,I_i} = \frac{1}{N_b} \sum_{(x,y)\in j_{th}block} \frac{1}{1+var(I_i(x,y))}, \tag{3.6}$$

where $I_i(x,y)$ is the intensity of image I_i at pixel (x,y), N_b represents the total number of pixels in the j_{th} block and $var(I_i(x,y))$ is the variance of three levels of neighborhood of the pixel (x,y). These features are used as an input of the neural network. The output of this network regarding each block represents the weighting factor of this block. They experimentally presented that their developed method achieves a high performance.

Chan *et al.* proposed another method to reduce the effect of image content details [Chan 2012]. The noise component was first extracted from each studied image using Block-Matching and 3D filtering method [Chierchia 2010] instead of wavelet based denoised filter since it shows better identification performance [Chierchia 2010]. The camera RPN was estimated using the maximum likelihood estimator. Then, the tested image is decomposed into blocks. For each block, the normalized correlation $\rho(b)$ and the predicted one $\hat{\rho}(b)$ are calculated, where b is the block index. So the normalized correlation of each image is:

$$\rho = \sum_{I\in M} \frac{\rho(b)}{M}, \tag{3.7}$$

where M is the number of blocks. The predicted correlation is:

$$\hat{\rho} = \sum_{I\in M} \frac{\hat{\rho}(b)}{M}, \tag{3.8}$$

$$\rho = H\theta, \tag{3.9}$$

where H is the block feature matrix. These features include three types (intensity, texture and signal flatting). θ is estimated using the least square estimator. Both the normalized correlation and the predicted one are served as an input of the SVM, and the output represents the digital source camera class. They experimentally showed that the identification accuracy is improved using their proposed 2D classifier.

3.2.4 Other PRNU applications

The specific properties of PRNU motivate other applications to be done in order to identify the imaging device. Khanna *et al.* based on the PRNU to identify the digital flatbed scanner [Khanna 2007]. In the spatial domain, they estimated the noise residual of RPN using the maximum likelihood estimator as a unique fingerprint. Then, they used an SVM classifier to classify the acquired image regarding the flatbed scanner class. This classifier achieved a better performance than the classical correlation measurement. Another work on digital flatbed scanner is presented in [Choi 2010]. The authors estimated the RPN in the frequency domain. Then, they detected its presence in any new image by Euclidean distance, taking into consideration that the source flatbed scanner has the minimum distance with the tested image. Fig. 3.4 illustrates an example of a digital flatbed scanner.

Figure 3.4: Digital flatbed scanner.

Away from the PRNU, there are other techniques to identify the source

device. For example Celiktutan *et al.* based on the fingerprint pattern created by the Color Filter Array (CFA) in order to identify the source cell phone camera [Celiktutan 2006]. They used an SVM classifier to classify the tested image according to the cell phone class. Kharrazi *et al.* presented a blind camera identification method in [Kharrazi 2004]. They classified the studied images regarding the source camera features. They extracted some color and quality features from the studied images, these features were the input vector of a classifier, and the classifier output refers to the studied camera class.

3.3 Medical device identification

When we turn toward the medical side, we cannot find many image forensics work. Huang *et al.* presented a first analysis of medical image forensics problem in [Huang 2012]. They proposed a method to detect whether a medical image has been modified or not. They used an SVM classifier with two groups of features as input. These features were extracted from the medical image. First group of features is the Histogram statistics of Recognized Block-based Discrete cosine transform coefficients (HRBD) [Shi 2005], these features correspond to the statistical moments of the Discrete Fourier Transform of one Histogram (DFTH) [Wang 2006]. The second group of features is the Histogram statistics of Reorganized Block-based Tchebichef moments (HRBT) [Liu 2009], they are extracted from the filtered version of DFTH [Wang 2006]. They experimentally verified the performance of their detection method on four modalities of medical images. These modalities were: MRI, CT-Images, X-ray and Ultrasound images. They were able to detect the falsification of these medical images with a good detection accuracy. In the direction to characterize the noise in CT-Scanner images for identification purposes, Solomon *et al.* compared image noise properties between two CT-Scanners from different manufacturers [Solomon 2012]. They based their

comparison on the noise texture. They characterize the noise texture using the Noise Power Spectrum NPS by computing the square of Fourier transform of the regions of interest in a uniform phantom[1]:

$$NPS(u,v) = \frac{d_x d_y}{N_x N_y}.|F[I(x,y) - P(x,y)]|^2, \tag{3.10}$$

where u and v are the spatial frequencies in the x and y directions, respectively, d_x and d_y are pixel size, N_x and N_y are the number of pixels in the x and y directions of the ROI, $F[]$ denotes the 2D Fourier transform, $I(x,y)$ is the pixel value of a ROI at position (x,y), and $P(x,y)$ is a 2^{nd} order polynomial fit of $I(x,y)$. Subtracting $P(x,y)$ from $I(x,y)$ reduces the low frequency artifacts in the NPS measure. They based on three steps to compare the convolution kernels between General Electric Scanner and Siemens one:

- Find the NPS of a uniform image reconstructed by each kernel.
- Filter the NPS by a human visual function.
- Compare the filtered NPS curves using both Root Mean Square Difference (RMSD) and Peak Frequency Difference (PFD) as similarity measurements.

Their experiments showed that NPS has the ability to differentiate two CT-Scanners of different manufacturers. But, this NPS cannot serve in case of two CT-Scanners models of the same manufacture. In addition that the specific conditions of extracting the NPS do not make it an ideal solution for CT-Scanner identification, since the NPS is calculated from an image of a homogeneous object for example.

Duan *et al.* proposed a method for medical device identification for digital radiography images [Duan 2014]. Their method is based on the pattern noise

[1]Phantom is a special designed object that is used to evaluate, analyze and tune the performance of medical imaging device.

model proposed by [Lukas 2006] to extract the RPN of digital radiography noise as an acquisition system fingerprint. To build the fingerprint of a digital radiography system, they averaged the noise residual of multiple image as follows:

$$RPN = \frac{1}{N}\sum_{i=1}^{N} n_i, \tag{3.11}$$

where n_i is the noise of digital radiography image, N is the number of images. To denoise the digital radiography image, they used a contourlet filtering [Satheesh 2011, Do 2005]. Then, they detect the presence of this fingerprint in any new digital radiography image based on the correlation value ρ:

$$\rho = corr(RPN, n) = \frac{cov(RPN, n)}{\sigma_{RPN}\sigma_n}, \tag{3.12}$$

where n is the noise of digital radiography test image and σ is a defined parameter. Then, the correlation value is compared with a manual threshold to decide whether this digital radiography image is identified correctly or not. They experimentally presented the ability of their method to identify the digital radiography acquisition system for a digital radiography test image. They verify their method on seven digital radiography systems and they were able to identify the source acquisition system with a high identification accuracy around 99%. But this work was applied only on the primitive 2D images of X-ray radiography.

Duan *et al.* presented a work on CT-Scanner identification [Duan 2015, Duan 2016]. They proposed to identify the CT-Scanner devices based on its reconstruction algorithm. They characterize the radial noise generated by CT-Scanner as a footprint, which is identified by the correlation between 180 directions of projection on 'Z' plane of the radial noise component and its average. They based on the classical method of [Lukas 2006] to extract the noise residual n:

$$n = s - F(s), \tag{3.13}$$

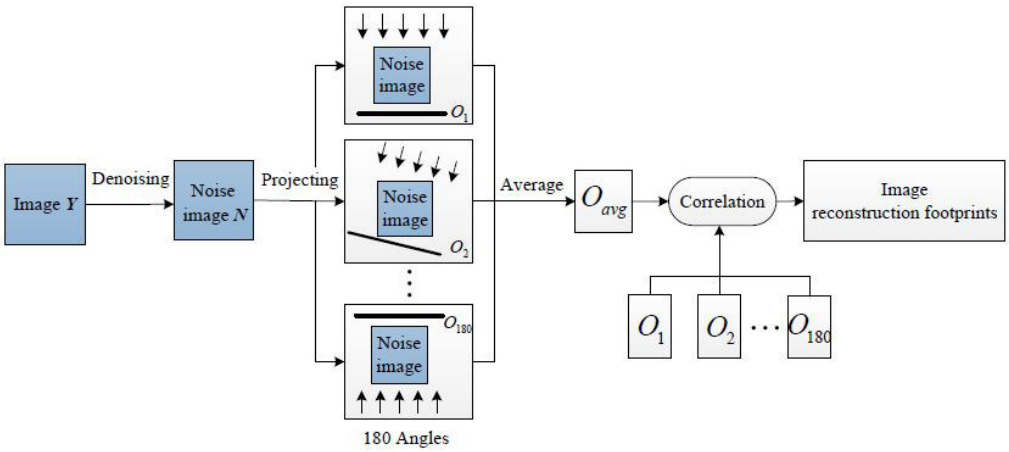

Figure 3.5: CT 3D image reconstruction algorithm footprint extraction.

where n is the image noise, s is the original image, and $F()$ is a wavelet based denoising method. Then, they estimated the noise of 180 angles and computed their average as follows:

$$\bar{p} = \sum_{j=1}^{180} p_j/180, \tag{3.14}$$

where $\bar{p}$ is the average of noise projections. Then, they computed the normalized correlations between 180 of noise projections and the averaged one $C(j)$:

$$C(j) = corr(\bar{p}, p_j) = \frac{(\bar{p} - \bar{\bar{p}}).(p_j - \bar{p_j})}{\|\bar{p} - \bar{\bar{p}}\|.\|p_j - \bar{p_j}\|}; j \in [1, 180]. \tag{3.15}$$

This 180 correlation values represent an image footprint as illustrated in Fig. 3.5

The resulted footprint vector C served as an input of an SVM classifier to classify the tested image regarding a set of CT-Scanners. They were able to validate their method based on their experiments by an accuracy about 95.04%. The basic limitation is to extract the noise using the classical method of [Lukas 2006], that will leave high frequency traces in addition to the noise. Moreover, applying an average on this set of projections enhances the high frequency traces, that will change the SVM classification to the anatomical

content level.

3.4 Conclusion

As we noticed, a lot of work has been done in the field of digital camera identification, most of them refers to [Lukas 2006], which is based on PRNU methods. Some improvements were applied to increase the identification accuracy. But when we turn to the medical side, we cannot find such amount of work in the medical device identification, and especially on CT-Scanner identification.

Chapter 4

CT-Scanner identification based on sensor noise analysis

Contents

4.1 Introduction

Regarding the different work on digital camera identification, most of the existing methods are basically based on the PRNU. PRNU-based identification methods achieved quite good results and identification performance. Moreover, in the analysis of CT-Scanner acquisition sensor and the camera imaging sensor, we noticed some kinds of similarities in the way of noise production and classification. Therefore, we propose to use PRNU-based method in the CT-Scanner identification.

In this chapter, we present a first analysis of CT-Scanner identification problem, that is aimed to authenticate the medical image information provided by DICOM file in order to identify its source. To do this, we ignore the DICOM header information and depend on the image content only. We assume that the CT-Scanner device left a fingerprint in each acquired image. This fingerprint is a unique one and related to the CT-Scanner model. The CT-Scanner fingerprint exists in the image noise, so we need to extract the noise from the CT-Scanner slices in order to extract its corresponding fingerprint.

We based on the identification method that is proposed in [Lukas 2006] to extract the Reference Pattern Noise (RPN) of the CT-Scanner as a unique fingerprint regarding its model. We describe how to extract this RPN from the CT-Scanner image content, then how to detect its presence in any new tested slice in order to authenticate its source information. We also provide some improvements on PRNU method, which consist of building a correlation map that gives an importance to each image pixel in order that the identification is based on the most important parts. Since the identification is basically related to the noise information, the core of our method is to extract the noise from the CT-Scanner slices, and we present a full description of the denoising method.

In Section 4.2 we present the CT-Scanner identification method based on the PRNU. In Section 4.3 we provide some improvements on the CT-Scanner identification method. The denoising method is presented in Section 4.4, and finally, we give a conclusion about this work in Section 4.5.

4.2 Identification based on sensor noise

We derive our work in CT-Scanner identification from the one presented in [Lukas 2006]. Our proposed method consists of extracting an RPN as a fingerprint of the CT-Scanner. Then, in the presence of many CT-Scanners with their fingerprints, we can measure the similarity between any new slice, and each fingerprint in order to authenticate the source CT-Scanner. We use the normalized correlation as a similarity metric. The tested slice is related to a specific CT-Scanner when it has a high correlation with its corresponding fingerprint. Fig. 4.1 gives an overview of the CT-Scanner identification method. In section 4.2.1 we present the CT-Scanner noise model. In Section 4.2.2 we explain how to extract the CT-Scanner RPN. Then, in Section 4.2.3 we provide the correlation as a similarity metric and when to decide the source CT-Scanner of a tested slice. Finally, experiments and discussions are presented in Section 4.2.4.

4.2.1 CT-Scanner noise model

From Section 2.3, and based on the sensor noise classification produced in [Lukas 2006, Goljan 2009], we can generalize the PRNU of CT-Scanner sensor pattern noise:

$$PRNU = PNU + EN, \tag{4.1}$$

and the CT-Scanner output model:

$$I = I_0 + I_0.Q + EN, \tag{4.2}$$

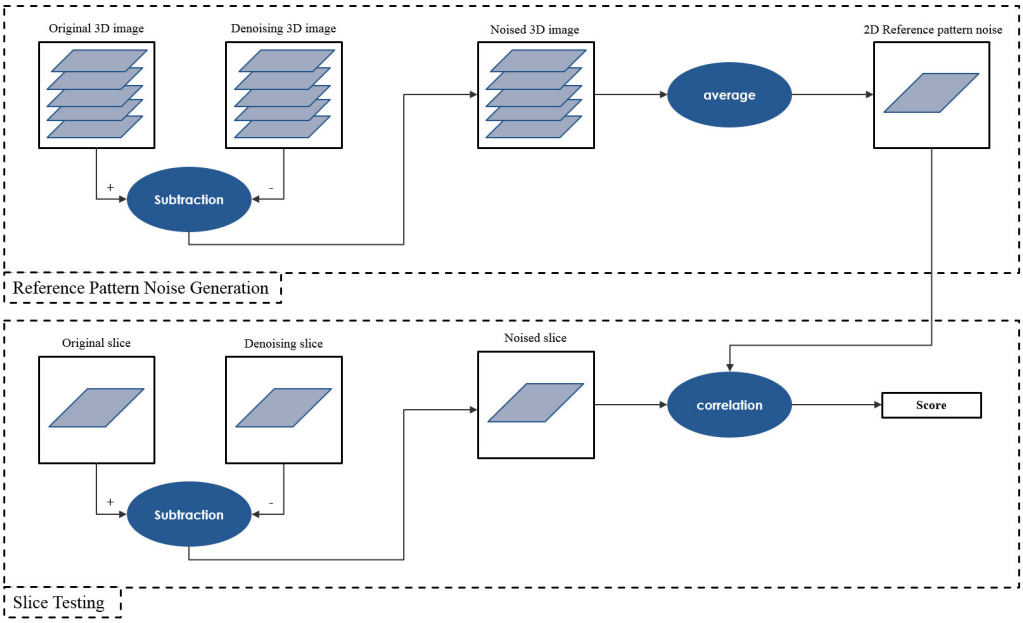

Figure 4.1: Identification method overview.

where I is the CT-Scanner reconstructed image, I_0 is the image content without any noise, Q is the quantum multiplicative noise, and EN is the electrical additive noise. The acquisition system of CT-Scanner keeps EN lower than Q noise, it is associated with only few x-rays. Consequently, it cannot characterize the sensor noise. So, we extract the CT-Scanner RPN, which characterizes the multiplicative factor Q of PRNU.

4.2.2 Building the CT-Scanner reference pattern noise

To build an RPN of a given CT-Scanner, we select a group of slices acquired by this CT-Scanner. Then, as illustrated in Fig. 4.2, we extract the noise component from the slice content. In order to extract the noise component, first we apply a denoising algorithm on the original slice to remove its noise residual. Then, we subtract the denoised slice from the original one to keep the noise residual only according to equation 4.2. This noise residual represents

the noise component of the given slice:

$$n^{(i)} = s^{(i)} - F(s^{(i)}), \tag{4.3}$$

where n is the noise component, s is the slice, $F()$ is the denoising function and i is the slice number. We are going to discuss in Section. 4.4 the detailed explanation about the used denoising method. Then, we apply an average operator on the slices of noise residual to build one 2D image that represents the CT-Scanner RPN or CT-Scanner fingerprint. This average step has two advantages:

1 Since the noise information exists in the high frequency, applying such average operator will enforce the noise information. Because the resulted noise component is about an aggregation of multiple noise slices.

2 Decreasing the random noise artifacts, that are exist in low frequencies.

The average operator is applied on the noise residual of the selected slices and gives an RPN as follows:

$$RPN = \frac{1}{N}\sum_{i=1}^{N} n^{(i)}, \tag{4.4}$$

where RPN is the reference pattern noise, N is the number of selected slices and n is the noise component of the CT-Scanner slice. This RPN represents the fingerprint of the given CT-Scanner. Fig. 4.2 illustrates an example of slice from a 3D image of phantom that is acquired by a Siemens

4.2.3 Decision by correlation

Correlation is the final step of this identification method to determine the source acquisition device. We applied the normalized correlation as a similarity measure between a CT-Scanner fingerprint and the noise component of

Figure 4.2: a) Example of an original slice (512x512) of a 3D image of phantom from Siemens device, b) Its denoised component, c) Its noise component.

any tested slice. The normalized correlation is calculated as follows:

$$corr(n_{(i)}, RPN) = \frac{(n_{(i)} - \bar{n_{(i)}}).(RPN - \overline{RPN})}{\|n_{(i)} - \bar{n_{(i)}}\| \|RPN - \overline{RPN}\|}, \tag{4.5}$$

where $\bar{n_{(i)}}$ is the average value of n, and $\overline{RPN}$ is the average value of RPN. To authenticate the source CT-Scanner of any tested slice, it should have the maximum correlation value among the different CT-Scanners RPN.

4.2.4 Experimental results

In this section we present the experimental results regarding the CT-Scanner identification method. In Section. 4.2.4.1 we preview the data we used in our experiments, and in Section. 4.2.4.2 we discuss the achieved results.

4.2.4.1 Data description

Experiments were applied on eight 3D images from 3 different CT-Scanners: Siemens 1, Siemens 2 and General Electric[1]. These images are coded in 16 bits and have similar acquisition parameters (Beam energy is (120, 140) Kv, pitch value is around 1 and the slice thickness is 3 mm). Fig. 4.3 illustrates

[1]From the two hospitals "CHU of Montpellier" and "Clinique du Parc" at Montpellier.

an example of 3D image of a phantom of Siemens 1, while Fig. 4.4 illustrates an example of 3D image of a phantom of Siemens 2, and Fig. 4.5 illustrates an example of 3D image of a phantom of General Electric.

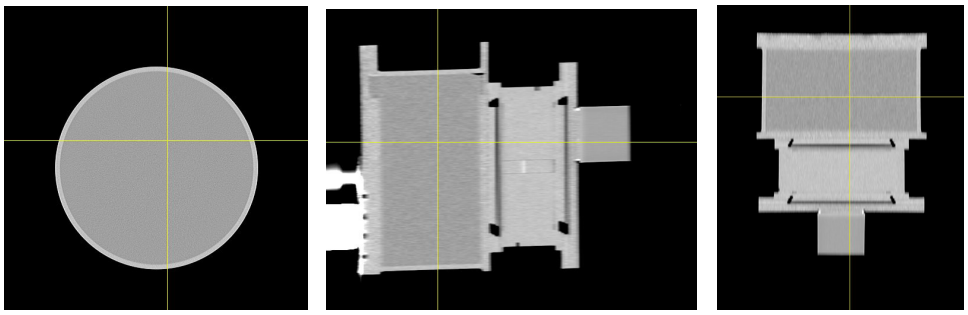

(a) Z slice (b) X slice (c) Y slice

Figure 4.3: Siemens 1: three slices of a 3D image of a phantom

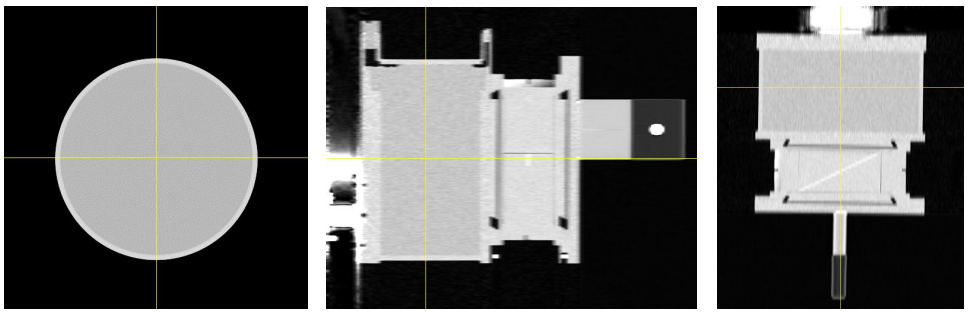

(a) Z slice (b) X slice (c) Y slice

Figure 4.4: Siemens 2: three slices of a 3D image of a phantom

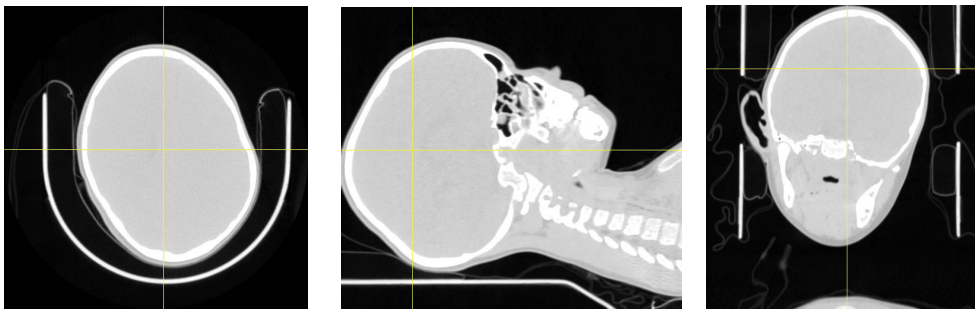

(a) Z slice (b) X slice (c) Y slice

Figure 4.5: General Electric: three slices of a 3D image of a head

We used three 3D images of a phantom from Siemens 1, three 3D images

of a phantom from Siemens 2 and two 3D images of a skull from General Electric. Each 3D image is composed of 100 slices, slice size is 512x512 pixels as illustrated in Table. 4.1.

Property/Model	Siemens 1	Siemens 2	GE
Content	phantom	phantom	skull
Nb of images	3	3	2
Nb of slices	300	300	200
Nb of slices of RPN	120	120	120
Nb of tested slices	180	180	80
Beam Energy	(120, 140)kv	(120, 140)kv	(120, 140)kv
Pitch Value	1	1	1
Size (pixels)	512x512	512x512	512x512
Bits per pixel	16	16	16
Slice thickness	3mm	3mm	3mm
Pixel size	1mm	1mm	1mm

Table 4.1: Characteristics of the experimental images.

4.2.4.2 Results and discussion

These experiments were applied on CT-Scanner slices. From each device, we selected randomly a group of 120 slices to build the RPNs following the procedure described in Section 4.2.2. Fig. 4.6 illustrates the three extracted RPNs regarding each device separately. In the RPNs, we can notice that some high frequency artifacts are caused by high frequency edges.

To verify the identification method, we selected a group of slices regarding each device in order to authenticate the source CT-Scanner information: 120 slices from the General Electric, 180 slices from the Siemens 1 and 180 slices from the Siemens 2. We extracted the noise component of each tested slice,

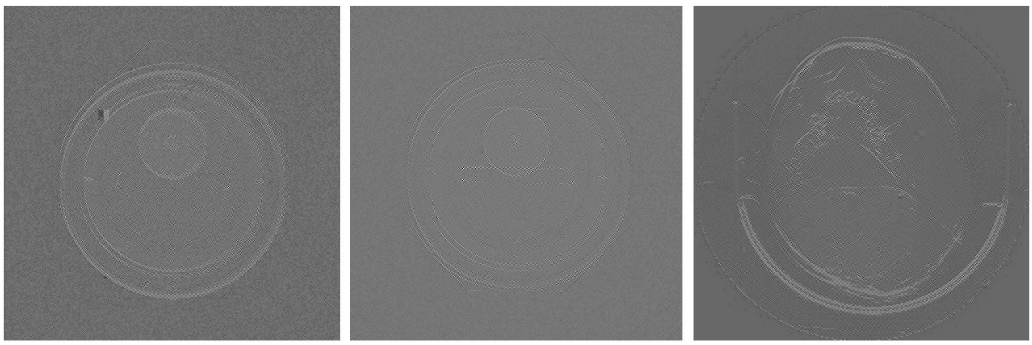

Figure 4.6: Example of the reference pattern noise from: a) the General Electric, b) The first Siemens device, c) The second Siemens device.

then we computed the normalized correlation to measure the similarity between each tested slice and each CT-Scanner RPN according to equation 4.5.

From plots in Fig. 4.7, Fig. 4.8 and Fig. 4.9, some correlation values are classified comparing to the other ones. These correlation values represent an indicator to the source CT-Scanner. As we defined, the correlation of a tested slice has a higher value with its device RPN.

The plot in Fig. 4.7 illustrates the correlation between three RPNs of three CT-Scanners (Siemens 1, Siemens 2 and General Electric) and the 180 slices from Siemens 1. The vertical axis represents the correlation value, and the horizontal one represents the slice number. From this plot, we can notice that correlation between the RPN of Siemens 1 and the tested slices of Siemens 1 has a quite higher values than the other ones. Almost all of these correlation values are more than 0.1, while all the other correlation ones are less. These correlation values represent the high similarity between this device RPN and the tested slice. However, we can consider the value 0.1 as a threshold that classifies the tested slices. We can decide that each tested slice has a correlation value superior to 0.1 was acquired by this device, otherwise, it was not. We can see the identification percent in Table. 4.2. The same remark can be

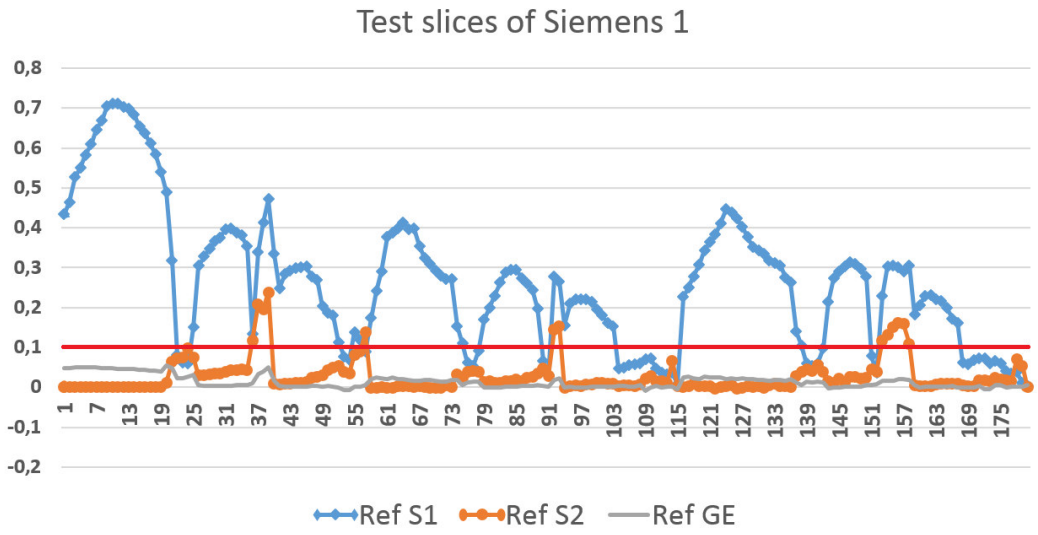

Figure 4.7: Correlations between the tested slices of Siemens 1 and the reference noise pattern regarding each device.

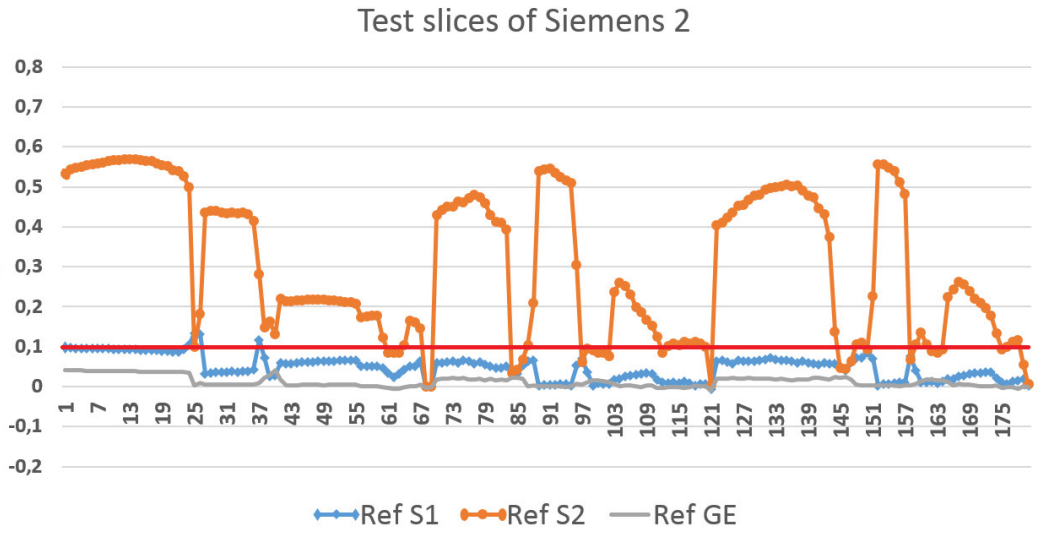

Figure 4.8: Correlations between the tested slices of Siemens 2 and the reference noise pattern regarding each device.

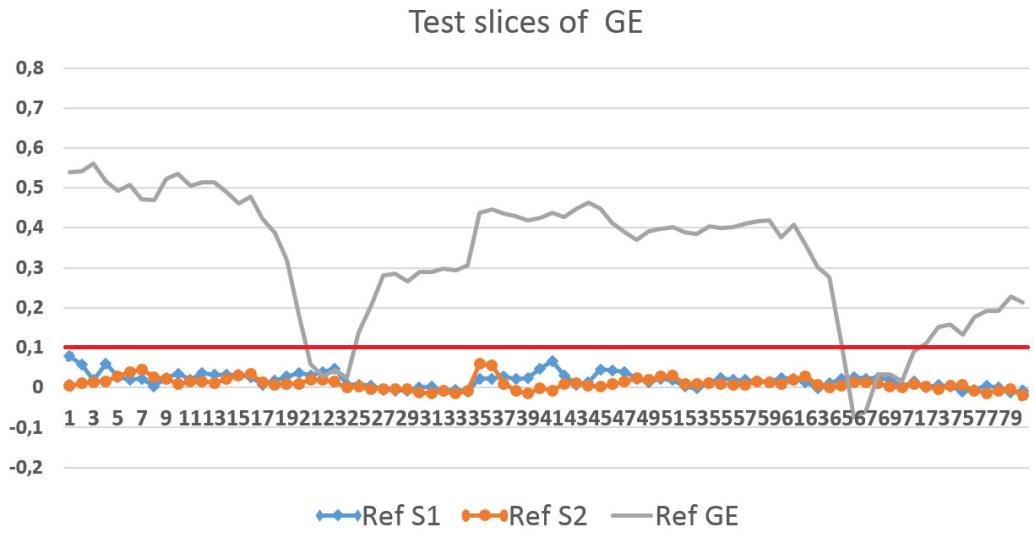

Figure 4.9: Correlations between the tested slices of General Electric and the reference noise pattern regarding each device.

applied on the plots of Fig. 4.8 and Fig. 4.9.

	Siemens 1	Siemens 2	GE
Siemens 1	**95.5 %**	3.0 %	5.0 %
Siemens 2	4.0 %	**97.0 %**	0
GE	0.5 %	0	**95.0 %**

Table 4.2: Identification accuracy

Table. 4.2 shows up the classification accuracy, when we correlated 180 slices from Siemens 1, 180 slices from Siemens 2 and 80 slices from General Electric with each device reference noise separately:

- 95.5 % of tested slices from Siemens 1 are classified correctly, while 4 % of them are classified as acquired by Siemens 2, and the rest 0.5% are classified as acquired by General Electric.

- 97 % of tested slices from Siemens 2 are classified correctly, while 3 %

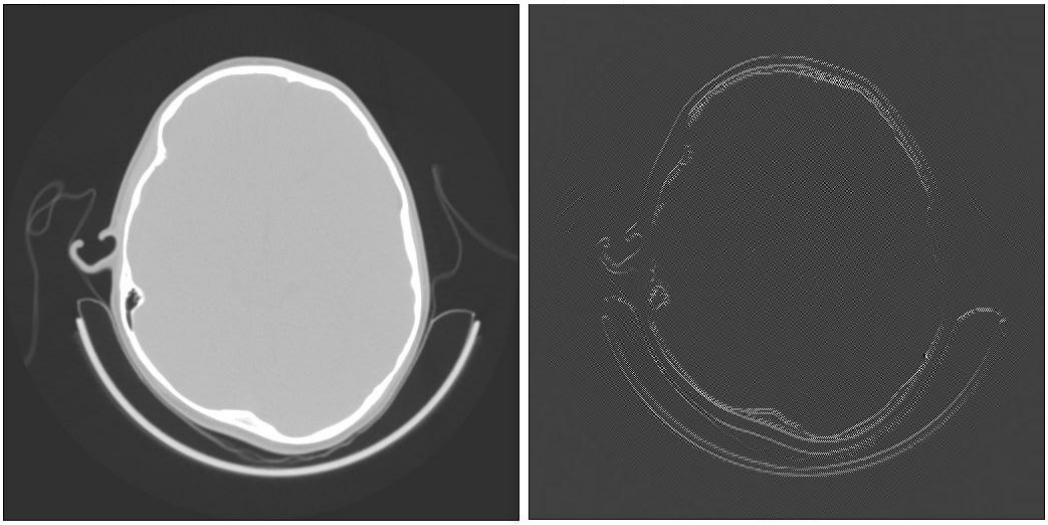

Figure 4.10: (a) Slice from a 3D image of a head from GE, (b) Its noise component.

of them are classified as acquired by Siemens 1.

- 95 % of tested slices from General Electric are classified correctly, while 5 % of them are classified as acquired by Siemens 1.

As the current CT-Scanner slices contain some anatomical parts. These anatomical borders create a signal in the noise slice. This signal exists in the form of artifacts in the area around the borders of the original slice. Fig.4.10 illustrates an example of one slice of a 3D image of a head from a General Electric device and its noise component.

These artifacts affect the identification performance and may turn it to the content level. Therefor, we have to differentiate the noise from high frequency artifacts. In the Section 4.3, we are going to improve the denoising algorithm by including a correlation map as suggested in [Chan 2013]. This correlation map takes into account the reliability of the noise computation at each pixel of the CT-Scanner slice. We are going to see also how to eliminate the high

frequency artifacts from the noise slice.

4.3 Improving sensor noise analysis

In this section, we present some improvements on the CT-Scanner identification method that was presented in Section 4.2. These improvements are basically composed of two parts. First part, enhancing the RPN extraction. Second part, building a correlation map that will associate to the RPN. This correlation map will give a weighting factor for each pixel of CT-Scanner testing slices. Then, we use the normalized correlation to measure the similarity also, but based on the correlation map. The source CT-Scanner will be still identified based on the highest correlation value. Fig. 4.11 illustrates the improved method of CT-Scanner identification, where we extract the RPN and the correlation map for each studied CT-Scanner, and they in their turn will associate to the correlation computation. In Section 4.3.1 we present

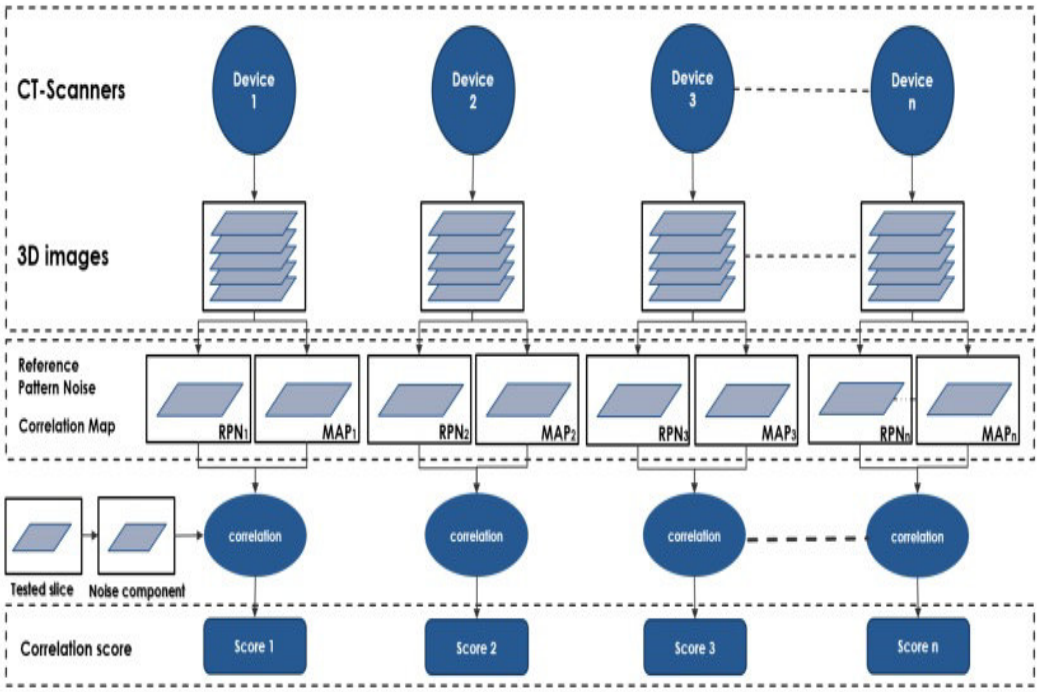

Figure 4.11: Improved identification method.

the method of noise extraction and correction regarding the new improved method. Then, in Section 4.3.2 we explain how to associate a correlation map to the new extracted RPN, and the decision of device identification is presented in Section 4.3.3. Finally, the experimental results are presented in Section 4.3.4.

4.3.1 Noise extraction and correction

To extract the noise component of CT-Scanner slice, we subtract the denoised slice from the original one based on the equation 4.3. But, in addition to the noise residual, we have another signal or component that remained in the high frequency. This signal exists as artifacts in the area around the edges of the original slice. In order to remove this kind of artifacts, we add a noise correction step. This step aims to detect the edges that exist in the original slice. Then, to mask them in the noised one, we apply an edge detection based on [Nitzberg 1993] as follows:

- Blur the original slice to remove the noise residual and high frequency information.
- Compute the gradient of each pixel of the blurred slice.
- Compute the norm of the gradient for each pixel.
- Finally, threshold the norm slice to extract the maximum local values that represent the edge mask.

Finally, we apply this mask on the previous noise component computed from equation 4.3:

$$n(i,j) = nn(i,j) \times mask(i,j), \tag{4.6}$$

where n is the pure noise component, nn is the normal noise component including the artifacts, and $mask$ is the edge mask. As a result, we have the pure noise component without any type of artifacts.

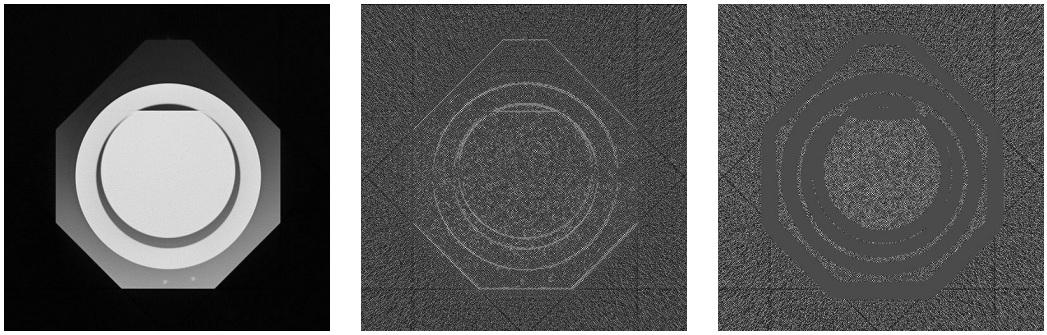

(a) (b) (c)

Figure 4.12: a) Example of a slice from CT-Scanner from Siemens, b) Its noise component, c) Its noise component without edges.

In Fig.4.12, we can see an example of a slice from a 3D image of phantom that was acquired by a Siemens device, where (a) is the original slice, (b) the normal noise component with artifacts, and (c) is the pure noise without any artifact.

4.3.2 Associating a correlation map to the RPN

The basic goal of the CT-Scanner RPN, as we already explained, is to provide an approximation of the CT-Scanner sensor noise output, since, the CT-Scanner acquisition system does not give a permission to access the raw data of the sensor output. We have seen in the section 4.2, that this approach removes the image content and keeps the noise only. Moreover, applying the average operator to extract the RPN will decrease the low frequency components and delete the random noise from the final RPN. Basically, the correlation map is built based on the same slices that were used to extract the CT-Scanner RPN. After selecting a group of slices, a CT-Scanner RPN is built according to Section 4.4. The selected slices belong to different 3D images, and the average is applied regarding 'Z' axis. In some slices, we removed artifacts from the noise residual. Consequently, according to pixel position, in some slices, the pixel

may belong to an edge and its information has been removed. So, this pixel position has lost some information regarding the 'Z' directional axis, while another pixel position did not lose any information since it does not belong to an edge. Based on the rule that non-edge pixel is more important that the edge one, we built a correlation map as suggested in [Chan 2013]. The correlation map gives information about the importance of each pixel according to its position. After selecting the RPN slices, we built the correlation map, where the pixel value represents its frequency as an edge in these slices:

$$map(i,j) = \sum_{I \in RPN slices} mask_I(i,j), \tag{4.7}$$

where map represents edge frequencies and $mask_I$ is the edge mask of I. In order to normalize the correlation map, we convert the values of the correlation map into percentage values, we inverted the map values and divided each pixel value by the maximum one. So each pixel value represents its importance regarding its frequency as an edge. The pixel with the highest edge frequency has a low importance and so it takes the value of 0, while the pixel with the lowest edge frequency has a high importance and it takes the value 1:

$$corr\_map(i,j) = \frac{Inv(map(i,j))}{max(map)}, \tag{4.8}$$

where $corr\_map$ is the final correlation map, $Inv()$ is the inversion factor and $max()$ is the maximum value of map.

4.3.3 Decision by correlation

The identification decision is also based on the similarity measurement of normalized correlation. The normalized correlation is computed between the noise component of a tested slice and the RPN of each given CT-Scanner. This normalized correlation is computed based on a weighting factor of the correlation map. So, we apply the correlation map on the RPN to extract the

weighted reference pattern noise $\widetilde{RPN}$:

$$\widetilde{RPN}(i,j) = RPN(i,j) \times corr\_map(i,j), \tag{4.9}$$

where RPN is the reference pattern noise and $corr\_map$ is the correlation map. We apply also the correlation map on the noise component to extract the weighted noise component $\tilde{n}$:

$$\tilde{n}(i,j) = n(i,j) \times corr\_map(i,j), \tag{4.10}$$

where n is the pure noise component and map is the correlation map. Finally, the correlation is:

$$corr(\tilde{n}_{(i)}, \widetilde{RPN}) = \frac{(\tilde{n}_{(i)} - \bar{\tilde{n}}_{(i)}).(\widetilde{RPN} - \overline{\widetilde{RPN}})}{\|\tilde{n}_{(i)} - \bar{\tilde{n}}_{(i)}\|\|\widetilde{RPN} - \overline{\widetilde{RPN}}\|}, \tag{4.11}$$

where $\bar{\tilde{n}}$ in the average value of $\tilde{n}$, $\overline{\widetilde{RPN}}$ is the average value of $\widetilde{RPN}$, and i is the slice number, the correlation is applied on the unmasked pixels only. The source CT-Scanner is identified based on the highest correlation value with its RPN.

4.3.4 Experimental results

In this section we present the experimental results regarding the improved CT-Scanner identification method. In Section. 4.3.4.1 we present the data we used in our experiments, and in Section. 4.3.4.2 we discuss the achieved results.

4.3.4.1 Data description

The experiments were applied on the same devices that were used in Section 4.2.4, but using more images. We used 40 3D images of 3600 slices from three different CT-Scanners: Siemens 1, Siemens 2 and General Electric.

These images have similar acquisition parameters as presented in Section 4.2.4. Fig. 4.13 illustrates an example of 3D image of a phantom of Siemens 1, while Fig. 4.14 illustrates an example of 3D image of a phantom of Siemens 2, and Fig. 4.15 illustrates an example of 3D image of a phantom of General Electric.

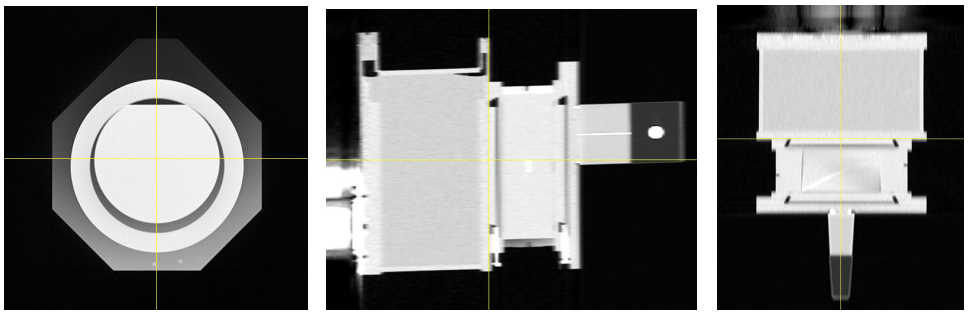

(a) Z slice (b) X slice (c) Y slice

Figure 4.13: Siemens 1: three slices of a 3D image of a phantom.

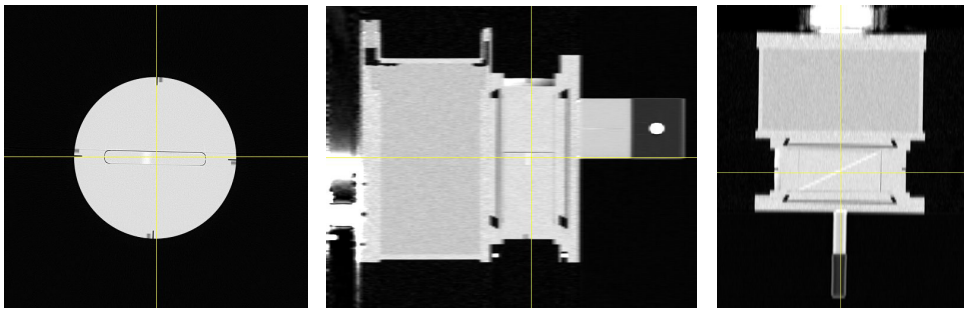

(a) Z slice (b) X slice (c) Y slice

Figure 4.14: Siemens 2: three slices of a 3D image of a phantom.

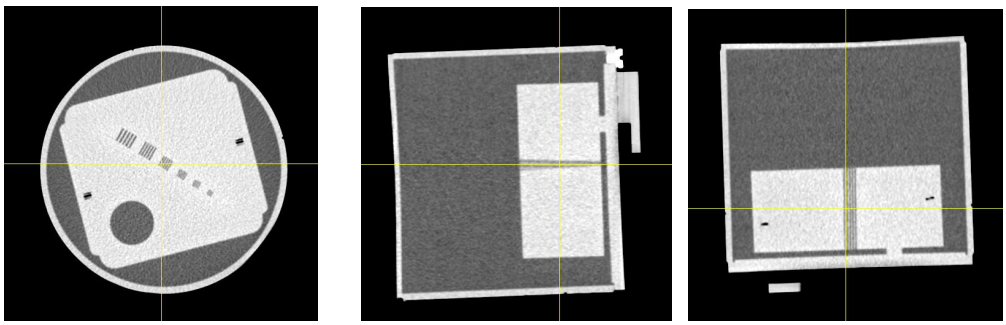

(a) Z slice (b) X slice (c) Y slice

Figure 4.15: General Electric: three slices of a 3D image of a phantom.

We used 12 3D images of phantom from Siemens 1, 12 3D images of phantom from Siemens 2 and 16 3D images of phantom from General Electric. Each 3D image is composed of almost 100 slices and the size of each slice is 512x512 as illustrated in Table 4.3.

Property/Model	**Siemens 1**	**Siemens 2**	**GE**
Content	phantom	phantom	phantom
Nb of images	12	12	16
Nb of slices	1200	1200	1200
Size (pixels)	512x512	512x512	512x512
Bits per pixel	16	16	16
Beam Energy	(120,140)kv	(120,140)kv	(120,140)kv
Pitch value	(0.5, 1)	(0.5, 1)	(0.5, 1)
Slice thickness	3mm	3mm	3mm
Pixel size	1mm	1mm	1mm
Nb of slices of RPN	200	200	200
Nb of tested slices	1000	1000	1000

Table 4.3: Characteristics of the experimental images.

4.3.4.2 Results and discussion

We apply our experiments on CT-Scanner slices. We select randomly 200 slices from each CT-Scanner to build the CT-Scanner RPN. Fig. 4.16 illustrates the RPNs of the three CT-Scanners. The correlation map is built also using the same slices that are involved in the RPN creation.

To build the correlation map, each pixel of the correlation map represents the frequency of its position as an edge in the selected slices. Fig. 4.17 illustrates the correlation maps of the three CT-Scanners. And the weighted RPN

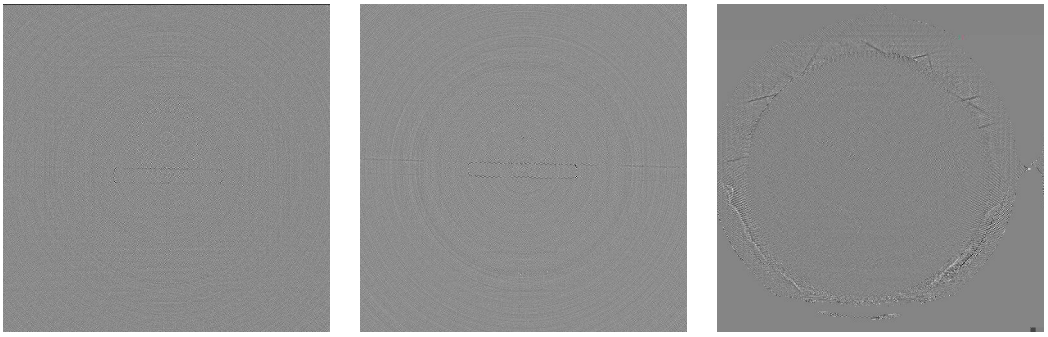

(a) RPN of S1 (b) RPN of S2 (c) RPN of GE

Figure 4.16: The reference pattern noise of each device.

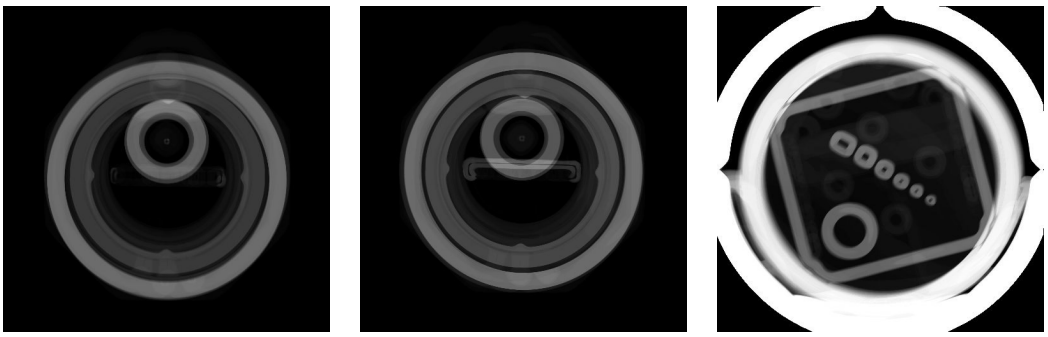

(a) Map of S1 (b) Map of S2 (c) Map of GE

Figure 4.17: The correlation map of each device.

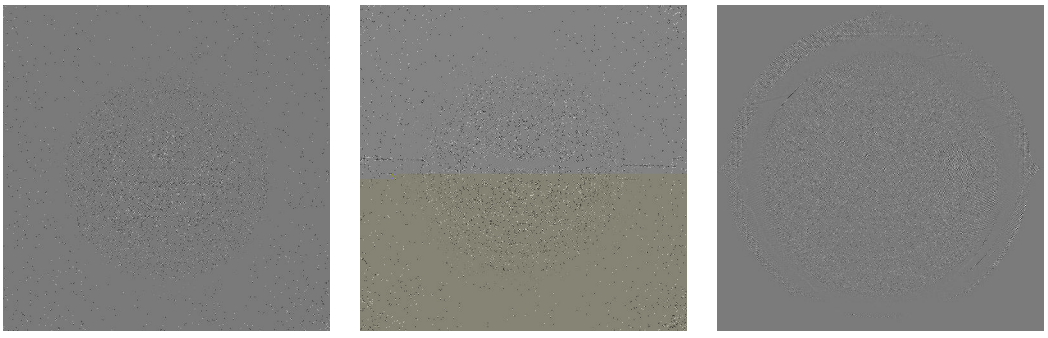

(a) RPN of S 1 (b) RPN of S 2 (c) RPN of GE

Figure 4.18: The three RPNs according to equation. (5.7).

of each CT-Scanner according to the equation 4.9 is illustrated in Fig. 4.18. In General Electric acquisition system, the acquired slice information is centered in a circle of diameter equal to the slice height or width. Therefor, we build a circle mask with a size equal to that of General Electric slice. In order to keep the same process region over all slices of all CT-Scanners, we applied this mask on all the processed slices. Finally, we calculated the normalized correlation between the noise component of the tested slices and the RPN of each device. This correlation depends on the correlation map as we declared in equations 4.9, 4.10 and 4.11.

The plots in Fig. 4.19, Fig. 4.20 and Fig. 4.21 represent the correlation between RPNs of three CT-Scanners and tested groups from each one. We can notice that correlation values between the tested slices and its corresponding source RPN are classified as higher values.

In the plot of Fig. 4.19 we can visualize the correlation between the RPNs of three CT-Scanners (Siemens 1, Siemens 2 and General Electric) and 1000 tested slices from Siemens 1. The horizontal axis represents the tested slice number and the vertical one represents the correlation value. It is clear in this plot that correlation between the tested slices and the RPN of Siemens 1 has higher values in comparison to the other ones. This correlation forms an evidence of the relation between these tested slices and its source RPN. So, we can decide that Siemens 1 is the source CT-Scanner of these tested slices. We can notice the same thing regarding the plots in both of Fig. 4.20 and Fig. 4.21.

Table 4.4 illustrates the identification accuracy of correlation between RPNs of the three CT-Scanners and 1000 tested slices from each one:

- 943 slices of Siemens 1 are classified correctly as acquired by Siemens 1, while 26 slices are classified as acquired by Siemens 2 and 31 slices as acquired by GE.

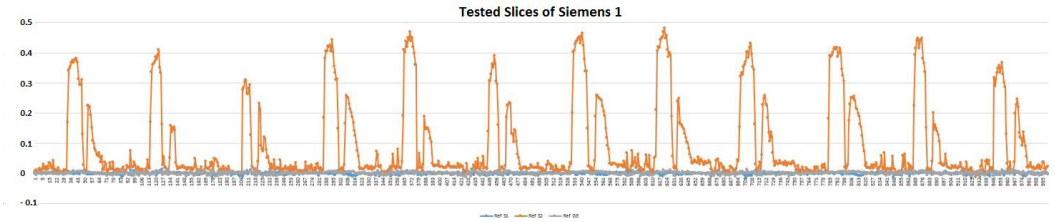

Figure 4.19: Correlation between 1000 tested slices of Siemens 1 and the RPN of each device.

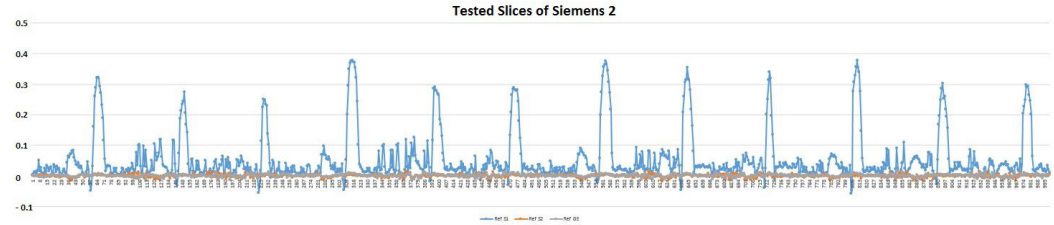

Figure 4.20: Correlation between 1000 tested slices of Siemens 2 and the RPN of each device.

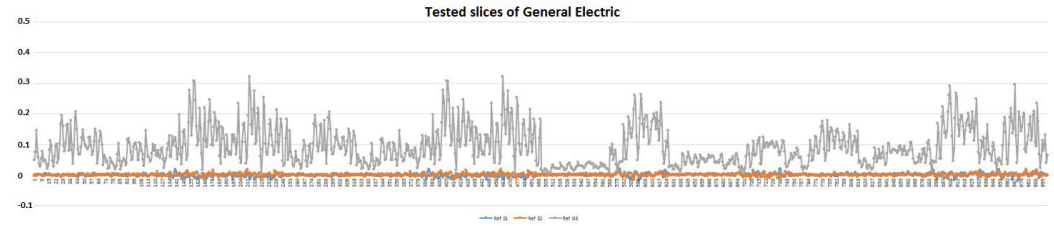

Figure 4.21: Correlation between 1000 tested slices of GE and the RPN of each device.

- 952 slices of Siemens 2 are classified correctly as acquired from Siemens 2, while 23 slices are classified as acquired by Siemens 1 and 25 slices as acquired by GE.
- 1000 slices of GE were classified correctly as acquired from GE.

	Siemens 1	**Siemens 2**	**GE**
Siemens 1	**94,3 %**	2,3 %	0 %
Siemens 2	2,6 %	**95,2 %**	0 %
GE	3,1 %	2,5 %	**100 %**

Table 4.4: Identification accuracy.

4.4 Denoising algorithm

Based on the work proposed in [Lukas 2006], we decide to use a wavelet-based Wiener filter [Choi 1998] since the noise component extracted this filter contains the minimum amount of scene traces (area around the edges in the noise image). Although that wavelet-based Wiener filter [Jacob 2004] provides good results, these results are obtained from the digital images which have quite smaller range of values than this in medical images. That was our motivation to apply some improvements on the CT-Scanner identification method in order to minimize the scene or anatomical traces that rest as artifacts in the high frequency. In this section, we present the wavelet-based Weiner denoising filter and its different parameters.

In the Wavelet domain, we applied a Wiener filter [Mihcak 1999, Kazubek 2003]. Basically, this algorithm is composed of two parts, the local variance estimation of the wavelet components in the first part and denoising of these components using Wiener filter [Jerhotová 2011] in the second one as follows:

- We compute four levels of wavelet decomposition [Burrus 1997]. In each level, we mark out the three high frequency sub-bands that are horizontal, vertical and diagonal. For four levels of wavelet decomposition with three sub-bands in each level we have 12 sub-bands for each processed image.

- For each wavelet sub-band, we use four levels of the pixel neighborhood. From the first boundary neighbors by a square size of (3x3) to the fourth boundary ones by a square size of (9x9), we apply the local variance estimation:

$$\hat{\sigma}_W^2(i,j) = max\left(0, \frac{1}{W^2}\sum_{(i,j)\in W*W}\left(X^2(i,j) - \sigma_0^2\right)\right), \tag{4.12}$$

  where $W \in \{3,5,7,9\}$ refers to the neighborhood level, X is the wavelet sub-band. σ_0 is an initial integer constant value that we tuned manually $\sigma_0 \in [1,6]$, in our experiments we selected the value of 3.

  Among the four previous values regarding the four levels of neighborhood, we select the minimum value as the estimated variance:

$$\hat{\sigma}^2(i,j) = min\left(\sigma_3^2(i,j), \sigma_5^2(i,j), \sigma_7^2(i,j), \sigma_9^2(i,j)\right). \tag{4.13}$$

- Denoise the wavelet sub-bands using Wiener filter, that is used to filter out noise that has corrupted a signal:

$$X_{den}(i,j) = X(i,j)\frac{\hat{\sigma}^2(i,j)}{\hat{\sigma}^2(i,j) + \sigma_0^2}, \tag{4.14}$$

  where X is the wavelet sub-band.

- Apply the inverse wavelet transformation on the denoised wavelet sub-bands to get the denoised component $F(s)$ of the original image s.

4.5 Conclusion

In this chapter, we proposed an analysis of CT-Scanner identification problem. Based on the state of the art, we presented our method to authenticate the CT-Scanner images and, to determine its source acquisition device. We extracted the CT-Scanner fingerprint from its output reconstructed images, then we

verified its presence in any new tested slice in order to validate its source. We can notice two advantages of extracting the CT-Scanner fingerprint in such way:

- It does not require an access to the sensor output, since we apply the identification steps on the reconstructed image directly.
- It can be applied on whatever model of CT-Scanner. For any new CT-Scanner model, we can build its RPN and include it in the identification dataset.

Since noise exists in the high frequency, the results of denoising method keep some high frequency artifacts in addition to noise. This fact encourages us to propose new improvements on the CT-Scanner identification problem which can keep the noise information only, enhance the identification performance and reduce the false alarm of identification. Our proposed improvements consist of masking the edges information in the noise slices and building a correlation map that increases the importance of unmasked parts and increases the identification accuracy from the other hand. Finally, we were able to identify the CT-Scanner based on its reconstructed slices. In Chapter 5, we are going to provide new solutions for CT-Scanner identification problem based on the specificity of medical images, and present a new fingerprint conception.

Chapter 5

New Directions for CT-Scanner Identification

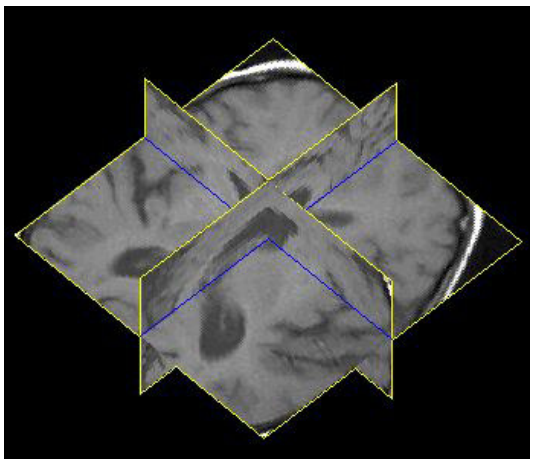

Contents

5.1 Introduction

We presented in Chapter 4 our first analysis of CT-Scanner identification problem. The proposed methods were based on the identification of digital camera. In this chapter, we present new methods for CT-Scanner identification based on the specificity of CT-Scanner images.

CT-Scanner images are reconstructed in three dimensions [Hu 1999]. Based on this principle, we propose a new fingerprint concept that takes into account the three dimensions of the CT-Scanner image. Regarding each dimension, we build a new identifier. This identifier is composed of an RPN and a correlation map. To identify the source of a tested slice, we measure the similarity between its noise component and each dimension identifier of each device. So, the CT-Scanner fingerprint consists of three dimension identifiers. This method allows the identification of both the CT-Scanner and the directional axis.

Another new concept is presented in this chapter, which is a separation into intensity "layers". We separate the CT-Scanner slice into three layers which correspond to the bone, the soft tissue and the air [Bui 2009]. Consequently, each CT-Scanner has three layer RPNs that constitute its fingerprint. To test any new slice, we measure the similarity between the noise component of each layer and its corresponding RPN of each device. The new experiments are applied on real data of patients.

In Section 5.2 we present the new CT-Scanner fingerprint of three dimension identifiers, and its effect on CT-Scanner identification. Then, in Section 5.3 we introduce the three layer RPNs fingerprint and the new identification method. Finally, we conclude our work in Section 5.4.

5.2 Extending the RPN to the different image axes

Since the CT-Scanner produces three dimension images, we propose to build an identifier along each axis. The traditional fingerprint we have proposed in Section 4.3 characterizes the noise only along 'Z' axis, that is the reconstruction axis of the CT-Scanner. But in case of attacking the original image by a simple rotation around 'X' or 'Y' directional axis, the previous RPN will not work anymore, because the noise along 'Z' axis does not take the same form as the noise along 'X' or 'Y' axes. However, the RPN which characterizes the noise along one axis, cannot characterize it along another one. It cannot even be used to authenticate the source information of slices which are not on the same axis.

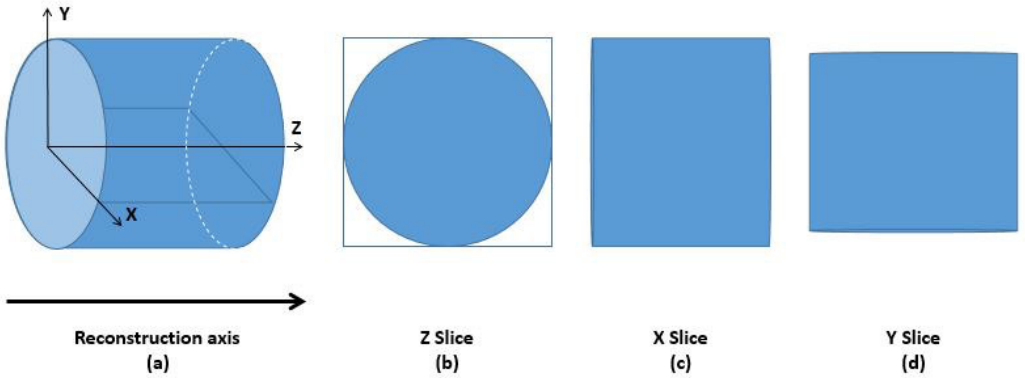

Figure 5.1: Noise form as a function of the directional axes.

Fig. 5.1 illustrates the form of generated noise along the reconstruction axis that is generally 'Z' axis. This generated noise takes a radial form along 'Z' axis according to the spiral or helical acquisition as presented in section 2.2. Consequently, it takes a horizontal cylinder form along 'X' axis, and a vertical cylinder one along 'Y' axis. The proposed method provides a new fingerprint concept. It consists of extracting a dimension identifier for each directional

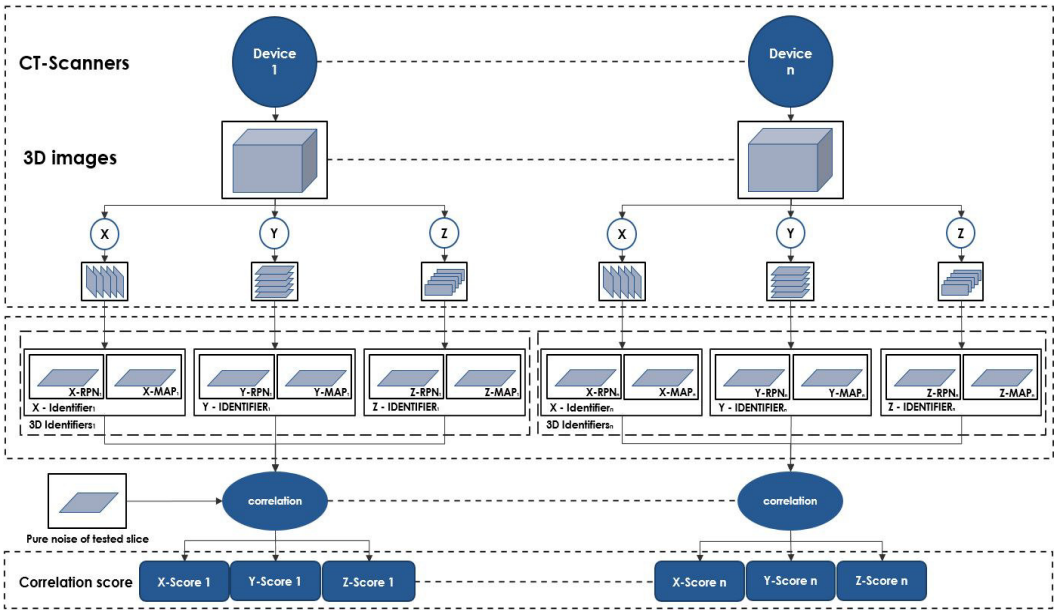

Figure 5.2: CT-Scanner identification method.

axis separately. Fig. 5.2 illustrates the new CT-Scanner identification method. In Section 5.2.1 we explain how to build a dimension identifier for a directional axis of a CT-Scanner. Then, we present in Section 5.2.2 how the identification criteria works. Finally, the experimental results are provided in Section 5.2.3.

5.2.1 Dimension identifier

The dimension identifier represents a unique fingerprint of the CT-Scanner regarding the directional axis, so it can be used to detect the directional axis of an unauthenticated tested image. As we have a 3D image, we can build an identifier for each directional axis: 'X' identifier, 'Y' identifier and 'Z' identifier as illustrated in Fig. 5.3. Each one of these identifiers is consisted of an RPN that characterizes the noise on this directional axis and a correlation map. Fig. 5.3 illustrates the applied schema on each studied CT-Scanner. Then, based on Section 4.3.1 and Section 4.3.2 we build the RPN and the correlation map of each dimension identifier along each directional axis. The same

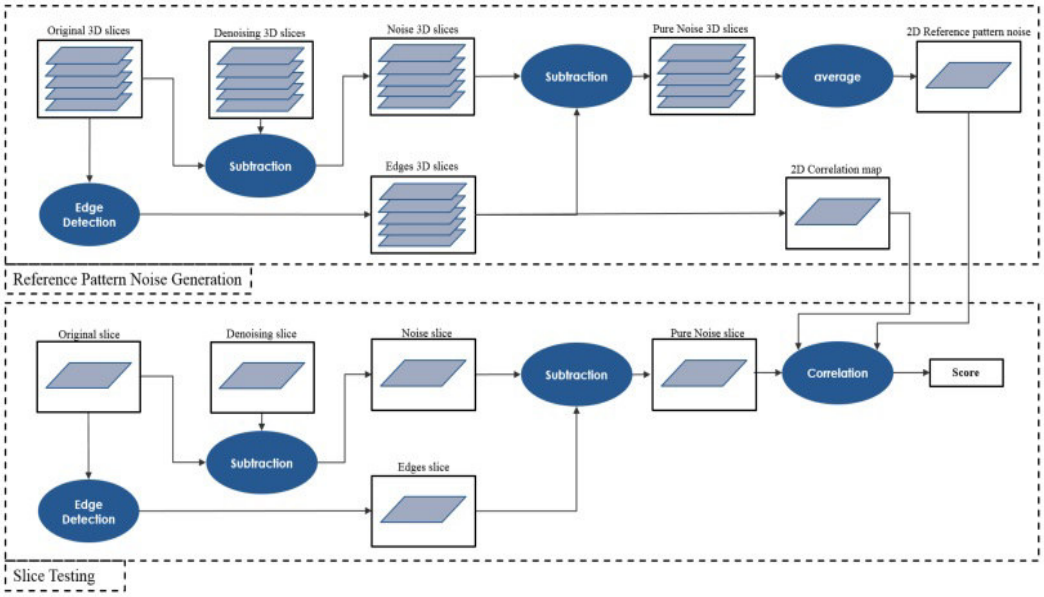

Figure 5.3: Identification method of each directional axis.

extraction schema that illustrated in Fig. 5.3 is applied along each dimension.

5.2.2 Identification by correlation

Now, for any new test slice, we can get two kinds of information. Firstly, its acquisition CT-Scanner, and secondly, its acquisition directional axis. The correlation step is applied on the three dimension identifiers of each CT-Scanner. This correlation is used to measure the similarity between a test slice and the CT-Scanner RPN. This correlation is calculated depending on the correlation map using the equation 4.11. The highest correlation value represents our guide to the source CT-Scanner and the directional axis.

5.2.3 Experimental results

In this section we present the experimental results using three dimension RPNs. In Section 5.2.3.1 we explore the used images in the experiments

and its characteristics. Then, in Section 5.2.3.2 we give our results and some discussions.

5.2.3.1 Data description

Experiments were applied on the same devices presented in Section 4.3.4 but with much more images. The three CT-Scanners are Siemens 1, Siemens 2 and General Electric. From each one we selected 10 3D images, each 3D image consists of 512 slices. A total number of 15,360 slices from the three CT-Scanners were used. All images have quite similar acquisition parameters (Beam energy: (120, 140) Kv, Pitch value: (0.5, 1), Reconstruction: (soft, hard)). Table 5.1 illustrates the characteristics of experimental images.

	Siemens 1	**Siemens 2**	**GE**
Content	phantom	phantom	phantom
Nb of images	10	10	10
Nb of slices	5,120	5,120	5,120
Size (pixels)	512x512	512x512	512x512
Bits per pixel	16	16	16
Slice thickness	1mm	1mm	1mm
Pixel size	1mm	1mm	1mm
Nb of slices of RPN	500	500	500
Nb of tested slices	500	500	500

Table 5.1: Characteristics of the experimental images.

We have initially the reconstructed images on 'Z' directional axis. We applied a resampling on 'Z' directional axis to create isotropic images of $1mm$, then we reformatted it on 'X', and 'Y' to create the same image on the three directional axes.

According to each directional axis, 100 slices were selected randomly from each image of each CT-Scanner. A totality of 1,000 slices according to each directional axis of each device were selected. 500 slices were selected to build the dimension identifier, and the other 500 slices were used to evaluate the identification performance.

5.2.3.2 Results and discussion

In Fig. 5.4 we can see an example of an original slice from a 3D image of phantom which is acquired by Siemens 1, slices from the three directional axes are illustrated. Fig. 5.5 illustrates the noise component of these slices.

In Fig. 5.5, it is clear that in addition to the noise, there are some high frequency artifacts that are result of edges. We masked the edges to remove these artifacts as we already explained in Section 4.3.2 and illustrated in Fig. 5.6 and Fig. 5.7.

To extract the RPN of each directional axis, we averaged 500 selected slices that contain noise only. Fig. 5.8 illustrates the three directional axes RPN of Siemens 1. The edge mask of the same selected slices is used to build the correlation map of each directional axis. As we mentioned before, the pixel value represents its position frequency as an edge in all slices. Fig. 5.9 illustrates the correlation maps of the three directional axes of Siemens 1. To measure the similarity between tested slices and different dimension identifiers, we calculated the normalized correlation between tested slices and the three dimension identifiers of each device. Based on the correlation map of each dimension identifier, we calculated the correlation between the noise component of the tested slice and the reference pattern noise. This correlation is computed directly, where there is almost no CPU time consumed.

Fig. 5.10, 5.11 and 5.12 illustrate the correlation values between each tested slice of each device and the dimension identifier of each one. In each plot, the 'X' axis represents the tested slice number and the 'Y' axis represents

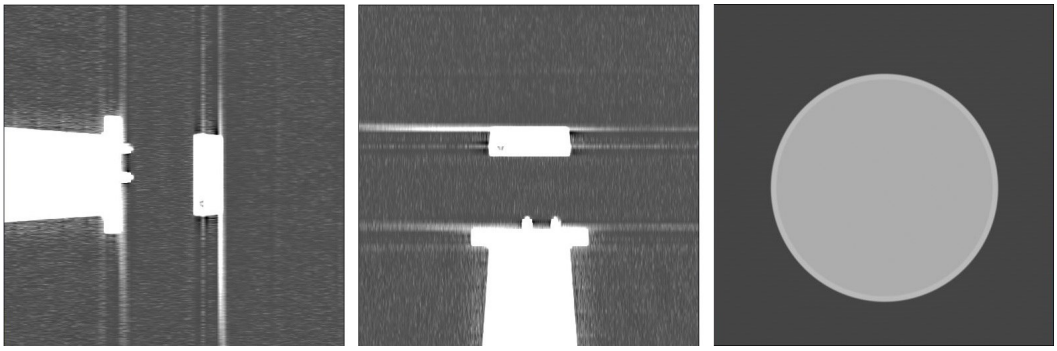

Figure 5.4: Original slices from Siemens 1 (X directional axis, Y directional axis, Z directional axis).

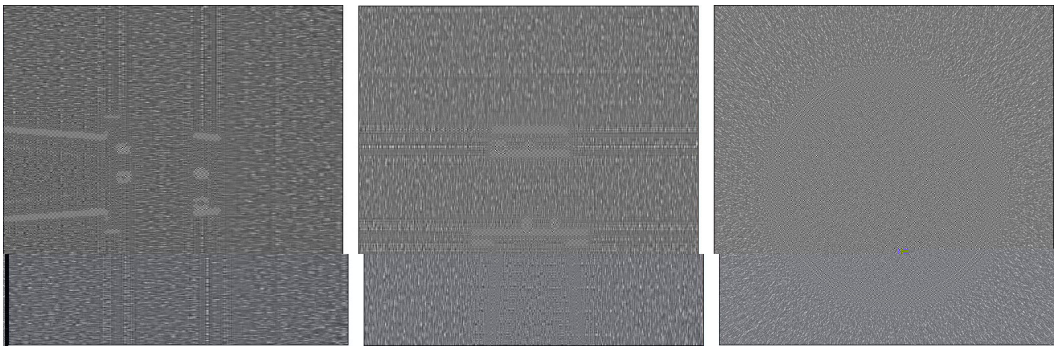

Figure 5.5: Noise component from Siemens 1 (X directional axis, Y directional axis, Z directional axis).

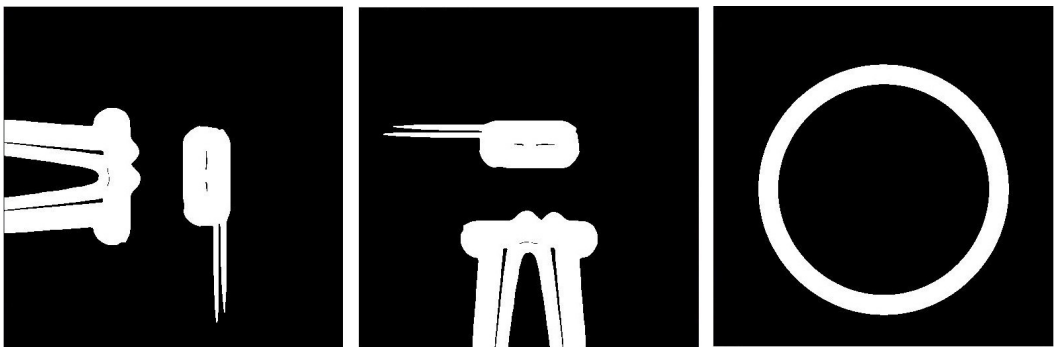

Figure 5.6: Edge mask from Siemens 1 (X directional axis, Y directional axis, Z directional axis).

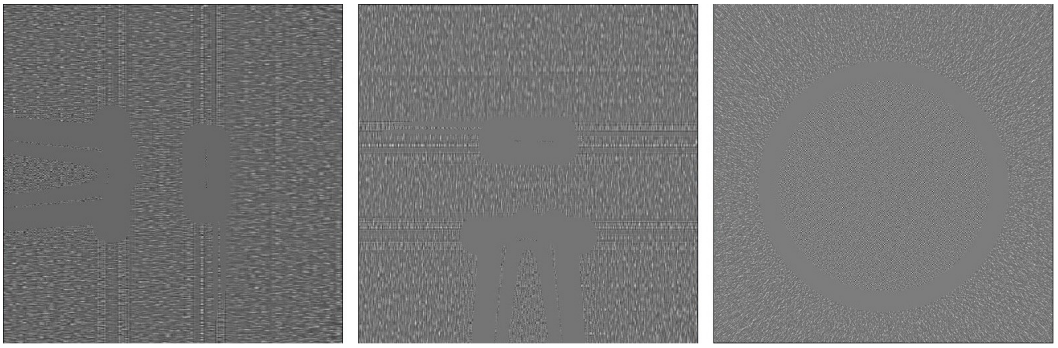

Figure 5.7: Pure noise component without traces from Siemens 1 (X directional axis, Y directional axis, Z directional axis).

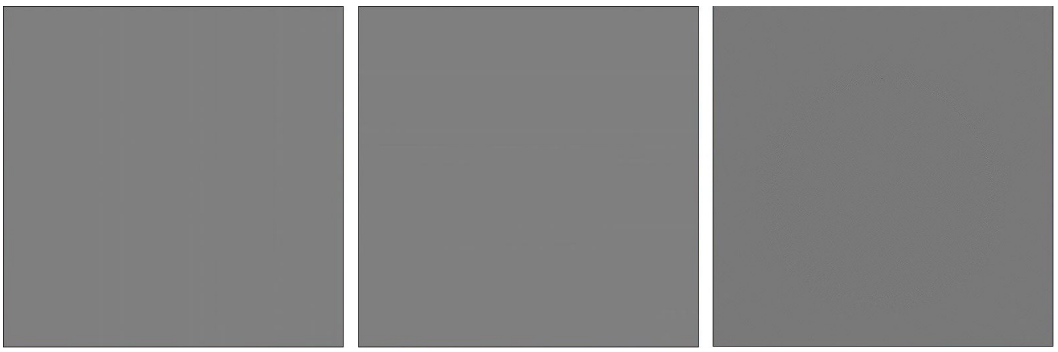

Figure 5.8: RPN of Siemens 1 (X directional axis , Y directional axis, Z directional axis).

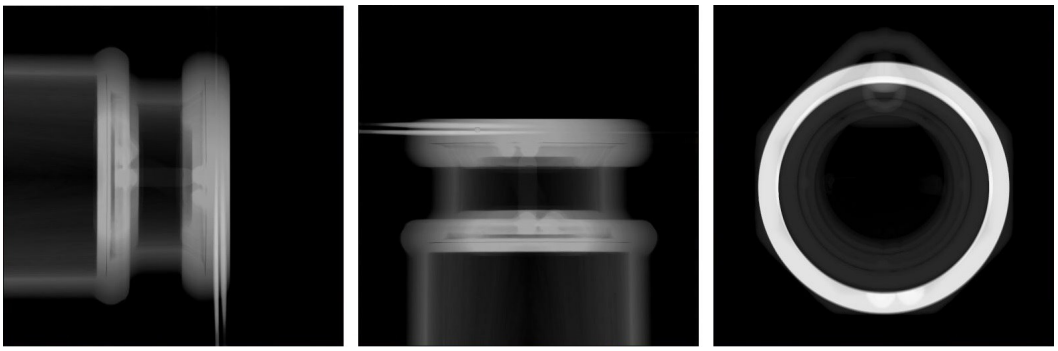

Figure 5.9: The correlation map from Siemens 1 (X directional axis , Y directional axis, Z directional axis).

the correlation value. We can notice that the correlation values between the tested slices and the dimension identifier of the same device and the same directional axis are always the highest.

From Fig. 5.10 and Table. 5.2, we notice that:

- (a) The best identification accuracy on 'X' axis is registered for Siemens 1, where 92.2 % of the tested slices are correctly classified as acquired from Siemens 1, and their directional axis is correctly identified as 'X'.
- (b) 88.6 % of the tested slices are classified correctly as acquired from Siemens 2, with correct directional axis.
- (c) 73 % of the tested slices are classified correctly as acquired from General Electric, with correct directional axis.

Moreover, most of the tested slices on 'X' axis that were not classified correctly in each tested group are associated with the same directional axis of another device:

- 5.8% of the tested slices from Siemens 1 on 'X' directional axis are associated with the 'X' axis of the Siemens 2.
- 9% of the tested slices from Siemens 2 on 'X' directional axis are associated with the 'X' axis of the Siemens 1.
- 6.6% of the tested slices from General Electric of 'X' directional axis are associated with the 'X' axis of the Siemens 2.

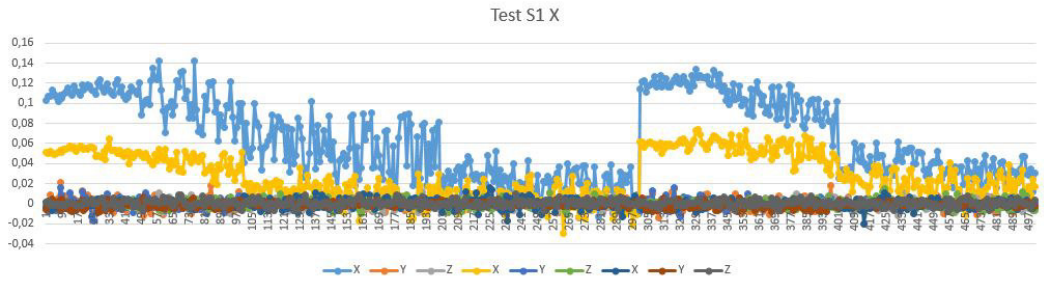

(a) Test slices from Siemens 1 and all the dimension identifiers.

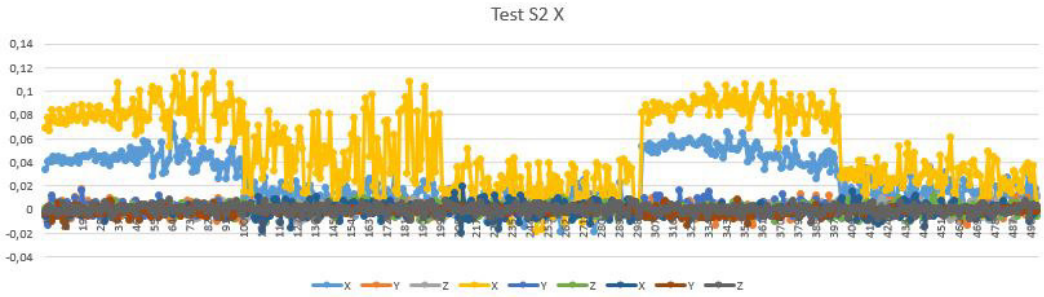

(b) Test slices from Siemens 2 and all the dimension identifiers.

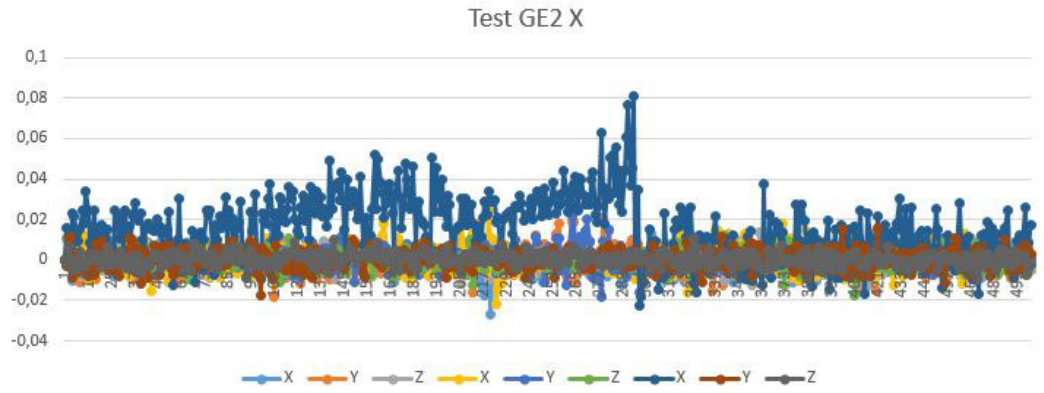

(c) Test slices from General electric and all the dimension identifiers.

Figure 5.10: Correlation between tested slices of 'X' directional axis from the three CT-Scanners and the three dimension identifiers of each one.

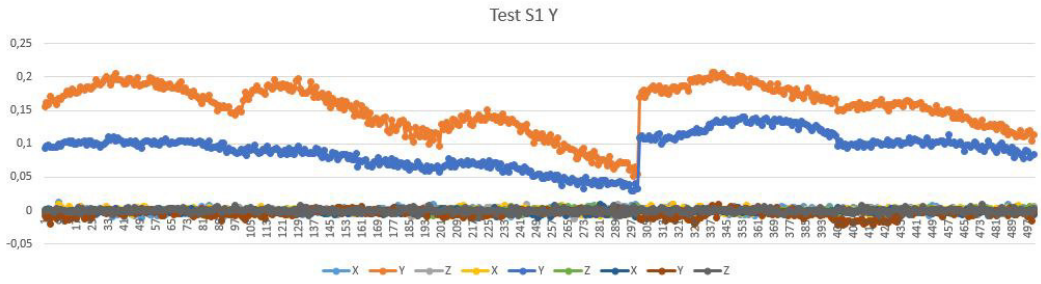

(a) Test slices from Siemens 1 and all the dimension identifiers.

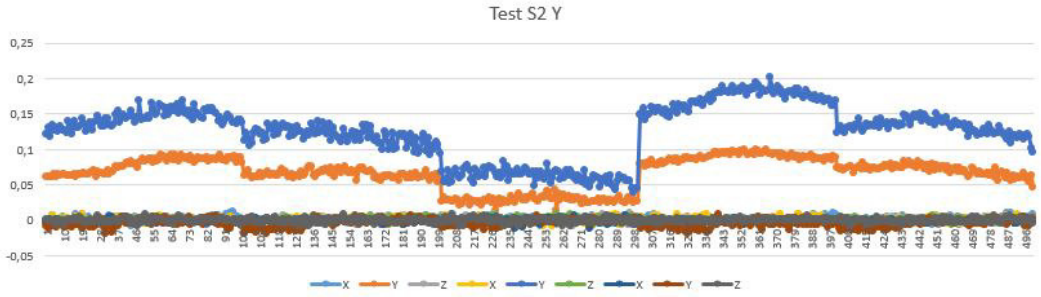

(b) Test slices from Siemens 2 and all the dimension identifiers.

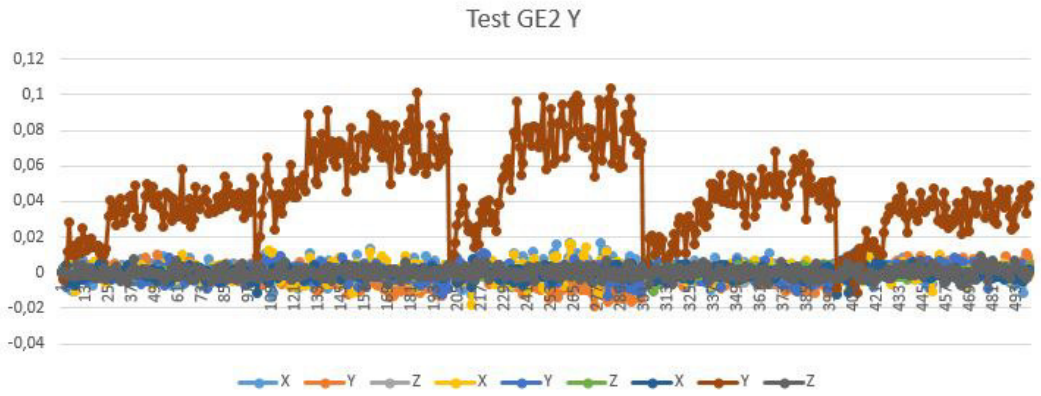

(c) Test slices from General Electric and all the dimension identifiers.

Figure 5.11: Correlation between tested slices of 'Y' directional axis from the three CT-Scanners and the three dimension identifiers of each one.

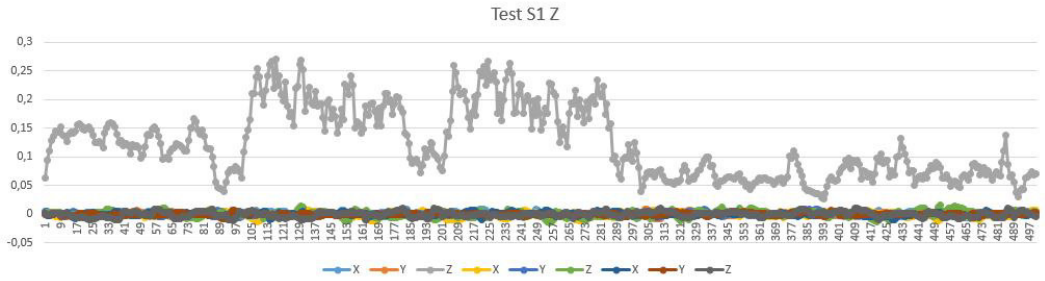

(a) Test slices from Siemens 1 and all the dimension identifiers.

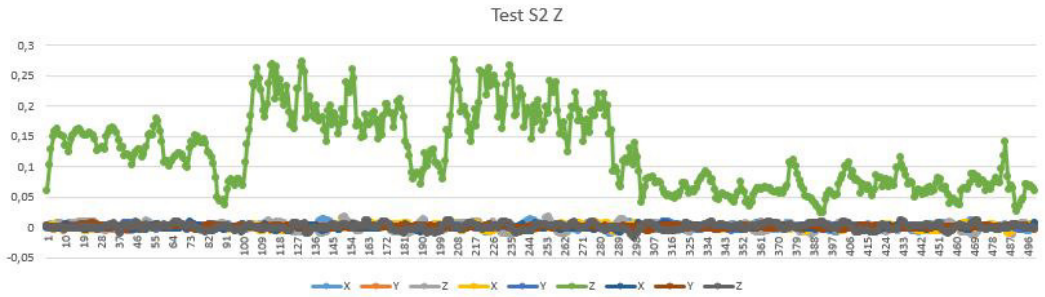

(b) Test slices from Siemens 2 and all the dimension identifiers.

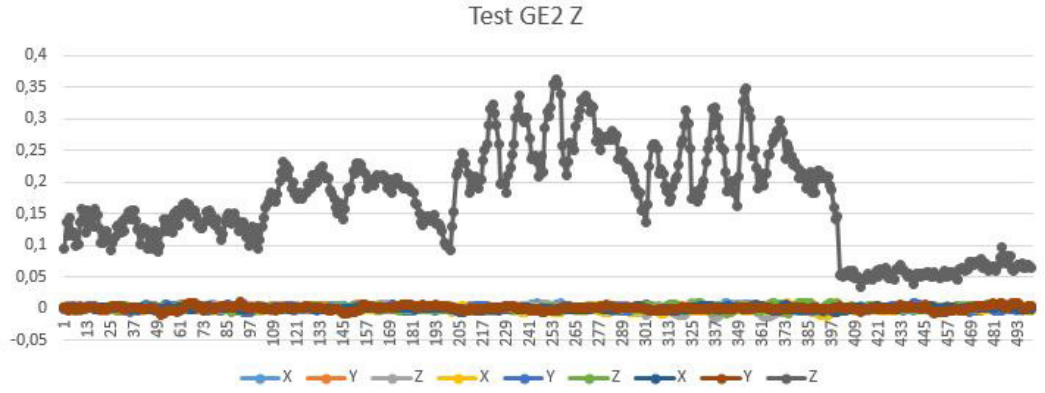

(c) Test slices from General Electric and all the dimension identifiers.

Figure 5.12: Correlation between tested slices of 'Z' directional axis from the three CT-Scanners and the three dimension identifiers of each one.

Ref \ Test	S1 Z	S1 X	S1 Y	S2 Z	S2 X	S2 Y	GE Z	GE X	GE Y
S1 Z	92,2 %	0	0	9 %	0	0	3,4 %	0	0
S1 X	0,2 %	100 %	0	0,2 %	0	0	1,8 %	0	0
S1 Y	0	0	100 %	0,2 %	0	0	3 %	0	0
S2 Z	5,8 %	0	0	88,6 %	0	0	6,6 %	0	0
S2 X	0	0	0	0	100 %	0	0,8 %	0,2 %	0
S2 Y	0,6 %	0	0	0,6 %	0	100 %	4,2 %	0	0
GE Z	0,4 %	0	0	0,8 %	0	0	73 %	0,2 %	0
GE X	0,4 %	0	0	0	0	0	4,4 %	99,6 %	0
GE Y	0,2 %	0	0	0,4 %	0	0	2,2 %	0	100 %

Table 5.2: Identification accuracy.

From Fig. 5.11 and Table. 5.2, we notice that:

- The identification accuracy is 100 %, where the source CT-Scanner is identified correctly for all the tested slices of the first Siemens and the second one, the 'Y' directional axis is identified correctly also.
- 99.6 % of tested slices are classified correctly as acquired from General Electric, and its directional axis is 'Y'.

From Fig. 5.12 and Table. 5.2, we notice that the identification accuracy is 100 %, where the source CT-Scanner is identified correctly for the three CT-Scanners on 'Z' directional axis. From Table. 5.2 also, we can notice that the identification on 'Y' and 'Z' axis, generally, is more accurate than 'X' axis.

5.3 Using an RPN of different intensity layers

The proposed identification method is based on extracting the CT-Scanner fingerprint. For each studied CT-Scanner, we build an RPN, this RPN is composed of three separated intensity layers. Using two thresholds [Sezgin 2004], we separate the studied slices into three intensity layers: air, soft tissue and bone. Then, regarding each layer, we extract the noise component and build its corresponding RPN. Finally, a correction step is applied on each layer RPN to remove any traces that left in the high frequency. Figure 5.13 illustrates the method overview. In Section 5.3.1 we explain how to separate into layers.

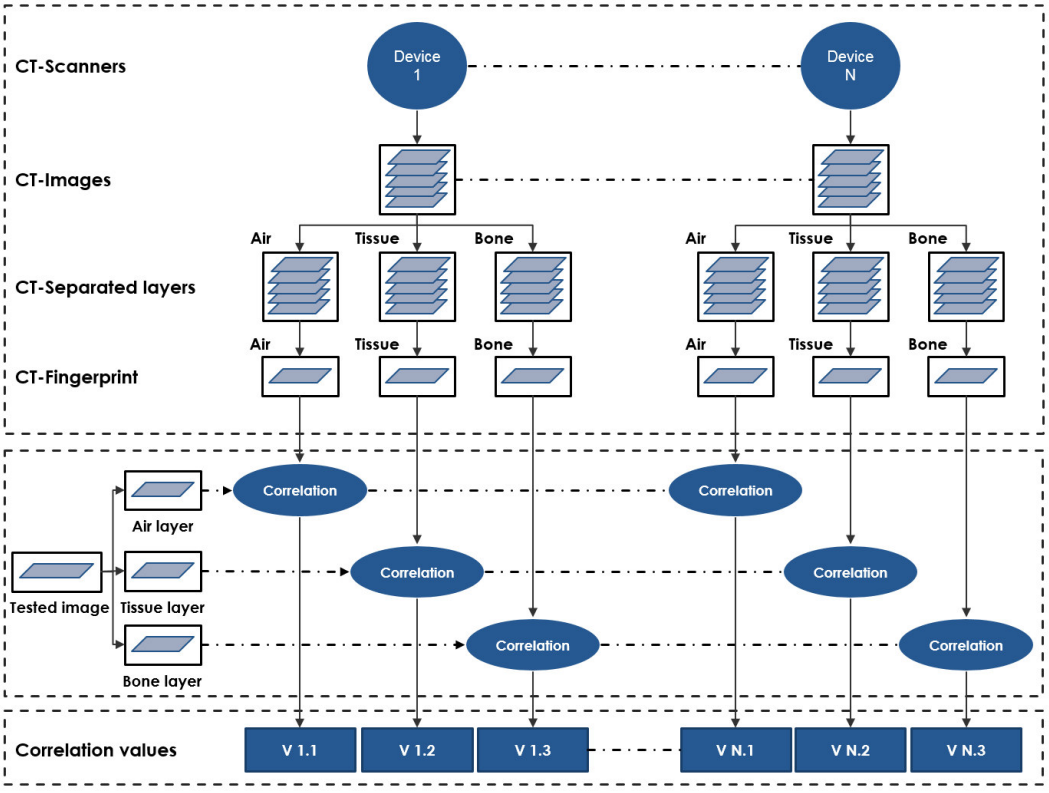

Figure 5.13: Identification method overview.

Then, we provide the noise extraction in Section 5.3.2, and the RPN extraction in Section 5.3.3. The new identification criteria is presented in Section 5.3.4. Finally, the experimental results are discussed in Section 5.3.5.

5.3.1 Separation into layers

The objective is to separate the CT-Scanner images into more homogeneous layers. Therefor, we can avoid any high frequency variation, that distorts noise extraction and analysis. Then we propose to decompose the CT-Scanner slice into 3 slices defined by 3 intensity layers: high-intensity areas that are the bones or contrast-enhanced anatomical structures, low-intensity areas that contain air-filled anatomical structures like lungs and average-intensity areas that correspond to soft tissue like muscle or fat. Then, we separate each studied slice into three layers using three ranges of intensities as follows:

$$\begin{aligned} A(i,j) &= s(i,j) | s(i,j) \in \ [a,b], \\ T(i,j) &= s(i,j) | s(i,j) \in \ ]b,c], \\ B(i,j) &= s(i,j) | S(i,j) \in \ ]c,d], \end{aligned} \tag{5.1}$$

where s is a CT-Scanner slice, A is the layer of air, T is the layer of soft tissue and B is the layer of bone. This separates all the intensities to the air value range [a,b], tissue value range]b,c] and bone value rang]c,d] respectively. These thresholds are defined based on the absolute Hounsfield scale [Hounsfield 1980] and were assessed over our experiments.
Based on the CT-Scanner noise model presented in Section 4.2.1, and equation 5.1, we can extend the form of the CT-Scanner image:

$$I = B + Q_B.B + T + Q_T.T + A + Q_A.A + EN. \tag{5.2}$$

With $I_1 = B$, $I_2 = T$ and $I_3 = A$, we have:

$$I = \sum_j (I_j + Q_j.I_j) + EN, \tag{5.3}$$

where: $j \in \{A, T, B\}$.

5.3.2 Noise extraction

The goal is to extract the noise component of each layer separately. We apply a denoising filter $F()$ described in Section 4.4 on the studied slice s_i. Then, we subtract the result from the original slice to extract the noise component based on equation 5.3 as follows:

$$rn_j = s_j - F(s_j), \tag{5.4}$$

where $j \in \{A, T, B\}$, rn_j is the preprocessed noise component. We noticed some additional low frequency by-products that rest with the noise, that are a result of denoising. To remove such kind of low frequency by-products from the studied slice, we apply the original layer binary mask B_j to keep this layer information, and to extract the final noise component n_i of this layer. This helps to avoid any low frequency by-products and keeps noise only:

$$n_j = B_j.rn_j. \tag{5.5}$$

5.3.3 Reference Pattern Noise

Here we apply the traditional RPN extraction method over the three separated layers, as follows:

1. Select a group of images, these images cover almost all the anatomical parts of the body. The image variety is an important point in building the RPN, in order to include all the noise variations regarding the different anatomical parts.

2. Separate the image slices into three layers, according to Section 5.3.1.

3. Extract the noise component of each layer, according to Section 5.3.2. The same problem of the high frequency artifacts is raised up here, where some traces are existed with the noise. The traces will increase

the false alarm of device identification and convert the identification to the content level as we already explained. Unlike the previous methods, we do not mask information in the high frequency, because the high frequency information is separated into its special layer, and is used to support the identification decision. So, we move to the frequency domain [Annadurai 2007] and apply a low pass wiener filter. This filter in its turn, removes such kind of artifacts, by suppressing its peaks and keep the enhanced RPN signal only.

4. Finally, we apply an average operation on the selected slices along each layer, to extract an RPN from each one:

$$RPN_j = \frac{1}{N_j} \sum_{i=1}^{N_j} n_{(j,i)}, \tag{5.6}$$

where $j \in \{A, T, B\}$, i is the slice number, N_j is the number of slices used in RPN creation and n_j is the noise component.

5.3.4 Identification criteria

The device identification is based on the similarity measure, where the noise of tested slice N_t should have a maximum similarity with RPN of the source CT-Scanner. The similarity between N_t and RPN is measured by the Peak-to-Correlation Energy (PCE), that is a more stable similarity metric than the normalized correlation and does not relate to the slice size [Goljan 2009, Goljan 2008a, Alfalou 2010]. PCE represents the ratio between the correlation peak height of the correlation plane, and the total energy of this plane, where the correlation plane is the cross-correlation between the two signals:

$$PCE(N_t, RPN_j) = \frac{E_p(N_t, RPN_j)}{E_{cp}(N_t, RPN_j)}, \tag{5.7}$$

where N_t is the noise component of the tested slice, RPN_j is the RPN of the tested layer according to the tested device, $j \in \{A, T, B\}$, E_p is the peak

height of the correlation plane and E_{cp} is the total energy of the correlation plane.

The PCE between the noise component of each tested separated layer and the RPN of the same layer is computed over all studied devices. To decide whether a slice belongs to a specific CT-Scanner, it should have the majority of its layers (in our proposed method, at least 2 layers out of 3) to be considered as coming from the same device.

5.3.5 Experimental results

In this section we present the experimental results regarding the three layer RPNs-based CT-Scanner identification. In Section 5.3.5.1 we preview the images used in the experiments and their characteristics. Then, in Section 5.3.5.2 we present the dataset preparation. Finally, in Section 5.3.5.3 we give our results and some discussions.

5.3.5.1 Data description

The experiments were applied on 60 3D images from new three different CT-Scanners (two Siemens S1, S2 and one General Electric GE). These images represent now real data of patients. A total number of 20,939 slices was used to build the RPN of the three devices and to validate the identification accuracy. These images cover almost all the anatomical body parts (head, abdomen, thorax, spine, neck, pelvic and chest). All of them have quite similar acquisition parameters (Beam energy: (100, 120, 140) Kv, Pitch value: (0.5, 1), Reconstruction: (soft, hard)). Table 5.3 illustrates the properties of the experimental images.

	S1	S2	GE
Nb of 3D images	20	20	20
Nb of slices	7,572	7,279	5,088
Size (pixels)	512x512	512x512	512x512
Bits per pixel	16	16	16
Nb of slices of RPN	3,363	3,756	2,092
Nb of tested slices	4,209	4,523	2,996

Table 5.3: Characteristics of the experimental images.

5.3.5.2 Dataset preprocessing

We separated each studied slice from our dataset into three layers. The separation threshold values were experimentally tested to validate its range, where the range values of air: [-990,-200], tissue:]-200,+200] and bone:]+200,+1500]. All the values below -990 or above the +1500 were ignored. Values below -990 are not important for our application, and the values above +1500 contain streak acquisition artifacts [Boas 2012]. Figure 5.14 illustrates an example of an original CT slice of a head and its three separated layers, it is from a 3D volume that was acquired by a Siemens 1. Then, we extracted the

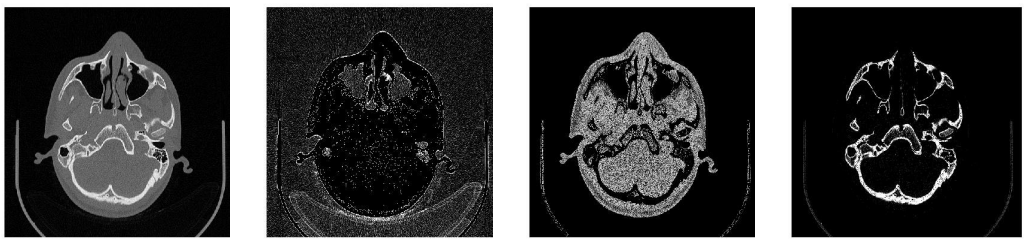

(a) Original (b) Air (c) Tissue (d) Bone

Figure 5.14: Original slice of a head and its three layers.

noise component of each slice, as we explained in Section 5.3.2. Figure. 5.15 illustrates an example of an original slice of a neck and the noise of its three layers. This slice, from a 3D volume has been acquired by a General Electric device.

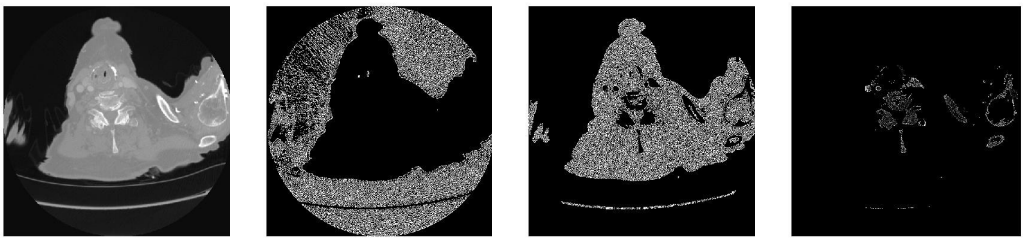

(a) Original (b) Air (c) Tissue (d) Bone

Figure 5.15: Original slice of a neck and the noise of its three layers.

Finally, from each device and each layer, we selected a group of slices to build the RPN according to equation 5.7. Fig. 5.16 illustrates three partial RPNs from three CT-Scanners using different layers.

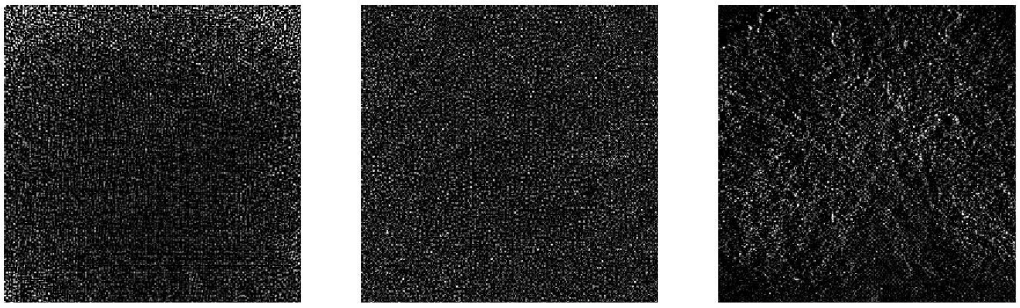

(a) S1: Air RPN (b) S2: Tissue RPN (c) GE: Bone RPN

Figure 5.16: RPNs from three different CT-Scanners and using different layers.

5.3.5.3 Results and discussion

The PCE is computed between noise component of each layer and RPN of each device from the same layer. Figure 5.17 illustrates examples of PCEs for three different layers, where x axis represents the slice number and y axis represents the PCE value.

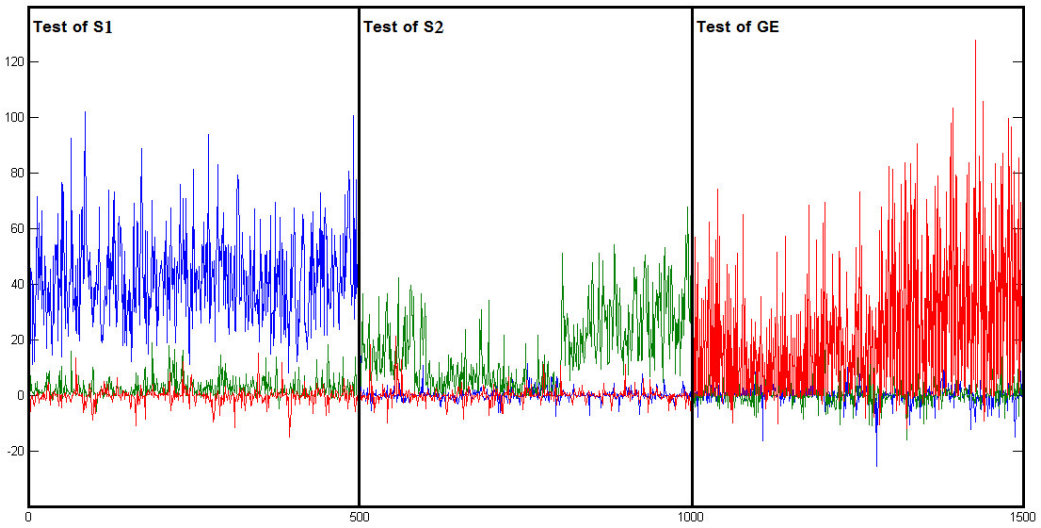

(a) PCEs from the tissue layer of the three CT-Scanners

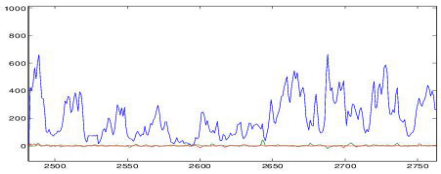

(b) PCEs from the bone of S1

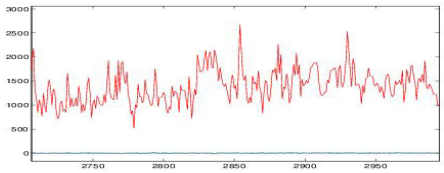

(c) PCEs from the air of GE

Figure 5.17: PCEs of tested slices from 3 CT-Scanners and 3 different layers.

In Fig. 5.17.a, an example of the correlation between 1500 slices (500 from each device respectively) and the three RPNs, regarding the soft tissue layer only. We notice:

- 0-500: slices from S1, they are classified correctly according to the highest PCE values (blue curve).
- 501-1000: slices from S2, they are classified correctly according to the PCE with RPN of the second Siemens scanner (green curve).
- 1001-1500: slices from GE, it is quite clear that the highest values of PCE also represent the correct classification of these slices (red curve).

In Fig. 5.17.b, the correlation of the **bone layer** only, between a partial tested group of S1 and the three RPNs of the three devices. We can identify the maximum PCE values according to the RPN of S1. In 5.17.c, the correlation of the air layer only, between the partial tested group of GE and the three RPNs of the three devices. The highest values of PCE with RPN of GE classify these slices correctly.

After defining the source CT-Scanner of each tested layer of all the tested slices according to Table 5.3, we can continue our identification criteria to identify the source CT-Scanner of each slice. To decide whether a given slice is correlated with a specific CT-Scanner, it should at least two of its layer are correlated with this CT-Scanner RPN. Table. 5.4 illustrates the identification accuracy of the separated layers.

Device \ Layer	**Air**	**Soft tissue**	**Bone**	**Majority**
Siemens 1	52 %	83 %	74 %	**81.32** %
Siemens 2	92 %	72 %	68 %	**83.63** %
GE	100 %	73 %	42 %	**81.81** %

Table 5.4: Identification accuracy matrix.

In Table 5.4 each row represents the identification accuracy of the separated layers of each device, the last column represents the percent of identification in case of two layers of the same slice are correlated with this device.

Table 5.5 illustrates the confusion matrix of the identification accuracy of the three CT-Scanners.

	Siemens 1	**Siemens 2**	**GE**	**No ID**
Siemens 1	**81.23** %	9.29 %	3.23 %	6.25 %
Siemens 2	4.75 %	**83.63** %	4.24 %	7.38 %
GE)	5.27 %	4.03 %	**81.81** %	8.89 %

Table 5.5: Confusion identification accuracy matrix.

In Table 5.5, each row represents the identification accuracy of each device, the last column represents the percent of slices that are not classified at all, since at least two layers are not well classified.

5.4 Conclusion and methods comparison

In this chapter, we proposed two advanced analyses for the CT-Scanner identification problem. Based on the specificity of medical CT-Scanner images, we presented two improvements on the CT-Scanner identification method to authenticate it.

Our advancements were concentrated on the fingerprint extraction level and the way it characterizes the noise. In the three directional RPNs, instead of avoiding the noise form on 'X' or 'Y' directional axes, we characterize the noise of each directional axis separately in its fingerprint, that help us to identify the CT-Scanner even if the image was acquired on other directional axis. Moreover advances were supported in the three layer RPNs, instead of masking or removing information in the high frequency as presented in the previous chapter, we used it to support the identification process. We characterized the noise of each layer in its fingerprint separately, that helps us to authenticate images even with high frequency information only.

Many advantages are carried out by these advanced methods, we increase the identification accuracy and decrease the false identification alarms. We were able to identify not only the acquisition CT-Scanner but also the acquisition directional axis. All of our experiments were applied on real data, and a quite high identification performance was achieved.

Finally, Table. 5.6 illustrates the comparison among our four proposed methods and two of the nearest ones for medical device identification, where:

- M1: Identification based on sensor noise, presented in Section 4.2.
- M2: Identification based on improving sensor noise analysis, presented in Section 4.3.
- M3: Identification of digital radiography image [Duan 2014].
- M4: Identification based on extending the RPN to the different axes, presented in Section 5.2.
- M5: Identification based on expanding the RPN into different layers, presented in Section 5.3.
- M6: Computed tomography image source identification [Duan 2015].

And Table. 5.7 illustrates the comparison among our four proposed methods according to he same dataset of test:

Property/Method	M1	M2	M3	M4	M5	M6
Authors	Kharboutly et al.	Kharboutly et al.	Duan et al.	Kharboutly et al.	Kharboutly et al.	Duan et al.
Year	2014	2015	2014	2015	2016	2015
Image type	CT	CT	Radiography	CT	CT	CT
Relevance to problem	Sufficient	Sufficient	Limited	Sufficient	Sufficient	Sufficient
Sensor noise based	Yes	Yes	Yes	Ye	Yes	No
Kind of method	PRNU	Improved PRNU	PRNU	Advanced PRNU	Advanced PRNU	Reconstruction footprint
Fingerprint	RPN	RPN and map	RPN	3D RPNs and map	3 layer RPNs	RPN
Denoising filter	Wiener	Wiener	Contourlet	Wiener	Wiener	Wiener
Number of tested images	8	40	234	30	60	3000
Number of tested slices	800	3,600	234	15,360	20,939	unknown
Minimum performance	95%	91.3%	99.9985%	73%	81.23%	84.95%
Maximum performance	97%	100%	99.999907%	100%	83.63%	99.24%
Real data	No	No	Yes	No	yes	Unknown

Table 5.6: Comparison of identification methods 1

Property/Method	M1	M2	M4	M5
Authors	Kharboutly et al.	Kharboutly et al.	Kharboutly et al.	Kharboutly et al.
Kind of method	PRNU	Improved PRNU	Advanced PRNU	Advanced PRNU
Fingerprint	RPN	RPN and map	3D RPNs and map	3 layer RPNs
Number of tested slices	20,939	20,939	20,939	20,939
Minimum performance	27%	31.3%	31.3%	81.23%
Maximum performance	37%	33.3%	33.3%	83.63%
Real data	yes	yes	yes	yes

Table 5.7: Comparison of identification methods 2

Chapter 6

Conclusion and perspectives

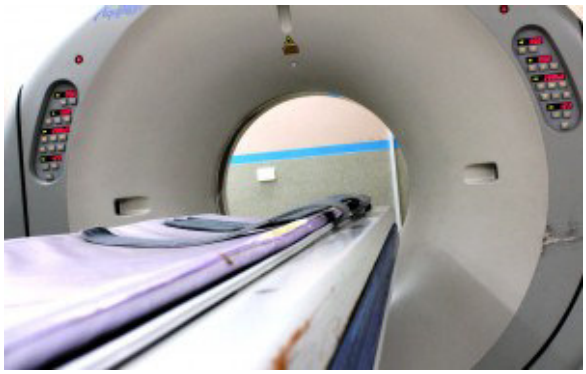

Contents

6.1 Conclusion

In the development of medical imaging devices and transmission solutions, the content security is always a critical issue. This thesis addresses an important problem in the domain of medical image forensics. It is about authenticating CT-Scanner images. Since these images are stored in DICOM format, and the DICOM header can be modified or deformed, we want to authenticate the acquisition device based on the image content.

Based on the literature, we proposed two groups of methods which analysis this kind of problems. In the first one, we proposed a CT-Scanner identification method by sensor noise analysis, where we built a fingerprint for a given CT-Scanner. Then, we detect its presence in the tested image to identify its source CT-Scanner. However, this fingerprint contained some scene traces, so we applied some improvements to remove such kind of artifacts and proposed a correlation map. The proposed correlation map aimed to give a weighting to the more important parts of the tested image. In the second group, we benefited from the two basic properties of medical images to produce two more advanced identification methods. First, we derived a new fingerprint, which consists of three dimension RPNs that aimed to identify the source directional axis in order to avoid the image attacking by rotating around different directional axes. Second, from the Hounsfield scale of intensity in CT-Scan images, we gave another new fingerprint that is composed of three layer RPNs.

Our experiments were applied on datasets of real CT-Scanners images of phantoms and patients, and on real images of patients. We were able to identify the CT-Scanners from its images and our proposed methods achieved quite high identification accuracy.

6.2 Perspectives

This thesis presents a research in medical image forensics. Many research tracks can be carried out in this domain in order to increase the identification performance as follows:

- Study other denoising filters [Zhong 2004, Li 2012, Satheesh 2011] and compare their results with the proposed one in this thesis. When we think about a new filter, we have to take in consideration two points: first, its behavior in extracting the noise and, second, its robustness with respect to scene traces.

- Generalize the identification method on 3D images, and study the case of extracting a 3D RPN in order to work with 3D images directly and not slices only.

- Associate the layer separation with the three dimension RPNs, in order to increase the performance of identifying the different axes of tested images.

- Study the influence of image compression [Barnsley 1993, Taubman 2012, Lewis 1992] on the identification method, especially in the case of lossy compression. Image compression is very important in medical images. We have to know whether the lost information will decrease the identification performance or not.

- Study the influence of image modification [Lehmann 1999] on the identification method. Image modification includes two cases. Firstly, modifying the image by mixing some slices from different images. This can be tested using the normal RPN, and when the tested slice has a low correlation with respect to the other ones. Secondly, modifying the slice

by mixing some parts from different slices. This can be tested by working with separated blocks [Strela 2001]. Then, we could detect the low correlation blocks and study their relevance with other RPNs of other devices.

- Study the situation of attacking such kind of CT-Scanner fingerprint [Caldelli 2011, Goljan 2011, Zhang 2012, Rosenfeld 2009]. If we insert an RPN of a given CT-Scanner in a falsified image, is it possible to detect its falsification or not.

Chapter 7

Résumé en français

Le traitement d'images médicales a pour but d'aider les médecins dans leur diagnostic et d'améliorer l'interprétation des résultats. Les scanners tomodensitométriques (scanners X) sont des outils d'imagerie médicale utilisés pour reconstruire des images 3D du corps humain. De nos jours, il est très important de sécuriser les images médicales lors de leur transmission, leur stockage, leur visualisation ou de leur partage entre spécialistes. Par exemple, dans la criminalistique des images, la capacité d'identifier le système d'acquisition d'une image à partir de cette dernière seulement, est un enjeu actuel. Dans cette thèse, nous présentons une première analyse du problème d'identification des scanners X. Pour proposer une solution à ce type de problèmes, nous nous sommes basés sur les méthodes d'identification d'appareils photo. Elles reposent sur l'extraction de l'empreinte des capteurs. L'objectif est alors de détecter sa présence dans les images testées. Pour extraire le bruit, nous utilisons un filtre de Wiener basé sur une transformation en ondelettes. Ensuite, nous nous appuyons sur les propriétés relatives aux images médicales pour proposer des solutions avancées pour l'identification des scanners X. Ces solutions sont basées sur une nouvelle conception de leur empreinte, cette dernière étant définie en trois dimensions et sur les trois couches: os, tissu et air. Pour évaluer notre travail, nous avons généré des résultats sur un ensemble de données réelles acquises avec différents scanners X. Finalement, nos méthodes sont robustes et donnent une précision d'authentification élevée. Nous sommes en

mesure d'identifier quelle machine a servi pour l'acquisition d'une image 3D et l'axe selon lequel elle a été effectuée.

Chapter 8

List of publications

- Internationales :

2014 CT-Scanner Identification based on Sensor Noise Analysis

Auteurs : Anas Kharboutly, William Puech, Gérard Subsol et Denis Hoa

European Workshop on Visual Information Processing

EUVIP - Paris, France

2015 Advanced Sensor Noise Analysis for CT-Scanner Identification from its 3D Images

Auteurs : Anas Kharboutly, William Puech, Gérard Subsol et Denis Hoa

IEEE International Conference on Image Processing Theory, Tools and Applications

IPTA - Orléans, France

2015 Improving Sensor Noise Analysis for CT-Scanner Identification

Auteurs : Anas Kharboutly, William Puech, Gérard Subsol et Denis Hoa

European Signal Processing Conference

EUSIPCO - Nice, France

- Nationales :

2014 Identification du Système d?Acquisition Scanner-X à partir de l'Analyse du Bruit dans des Images Médicales

Auteurs : Anas Kharboutly, William Puech, Gérard Subsol et Denis Hoa

Colloque CORESA (COmpression et REprésentation des Signaux Audiovisuels)

CORESA - Reims, France

2016 Identification du Scanner X à partir d?Empreintes du Capteur

Auteurs : Anas Kharboutly, William Puech, Gérard Subsol et Denis Hoa

Colloque CORESA (COmpression et REprésentation des Signaux Audiovisuels)

CORESA - Nancy, France

Bibliography

[Alfalou 2010] Ayman Alfalou and Christian Brosseau. *Understanding correlation techniques for face recognition: from basics to applications*. Face Recognition, pages 353–380, 2010. (Cited on page 85.)

[Annadurai 2007] S Annadurai. Fundamentals of digital image processing. Pearson Education India, 2007. (Cited on page 85.)

[Barnsley 1993] Michael F Barnsley and Lyman P Hurd. Fractal image compression. AK Peters, Ldt., 1993. (Cited on page 97.)

[Beister 2012] Marcel Beister, Daniel Kolditz and Willi A Kalender. *Iterative reconstruction methods in X-ray CT*. Physica medica, vol. 28, no. 2, pages 94–108, 2012. (Cited on page 14.)

[Benseler 2006] JS Benseler. The radiology handbook: A pocket guide to medical imaging, volume 2. Ohio University Press, 2006. (Cited on page 8.)

[Beutel 2000] Jacob Beutel, Harold L Kundel and Richard L Van Metter. *Handbook of Medical Imaging, volume 1: Physics and Psychophysics*. 2000. (Cited on page 2.)

[Bidgood 1997] W Dean Bidgood, Steven C Horii, Fred W Prior and Donald E Van Syckle. *Understanding and using DICOM, the data interchange standard for biomedical imaging*. Journal of the American Medical Informatics Association, vol. 4, no. 3, pages 199–212, 1997. (Cited on page 3.)

[Boas 2012] F Edward Boas and Dominik Fleischmann. *CT artifacts: causes and reduction techniques*. Imaging in Medicine, vol. 4, no. 2, pages 229–240, 2012. (Cited on page 87.)

[Brown 2008] Kevin John Brown, David Jaffray, Jeffrey H Siewerdsen, Marcel Van Herk and Jan-Jakob Sonke. *Computed tomography scanning*, April 8 2008. US Patent 7,356,112. (Cited on page 12.)

[Bui 2009] Alex AT Bui and Ricky K Taira. Medical imaging informatics. Springer Science & Business Media, 2009. (Cited on page 69.)

[Burrus 1997] C Sidney Burrus, Ramesh A Gopinath and Haitao Guo. *Introduction to wavelets and wavelet transforms: a primer*. 1997. (Cited on page 63.)

[Bushberg 2011] Jerrold T. Bushberg, J. Anthony Seibert, Edwin M. Leidholdt Jr. and John M. Boone. The essential physics of medical imaging, third edition. LWW, third, north american edition édition, 12 2011. (Cited on pages 8 and 16.)

[Caldelli 2011] Roberto Caldelli, Irene Amerini and Andrea Novi. *An analysis on attacker actions in fingerprint-copy attack in source camera identification*. In 2011 IEEE International Workshop on Information Forensics and Security, pages 1–6. IEEE, 2011. (Cited on page 98.)

[Celiktutan 2006] O. Celiktutan, İ. Avcibaş, B. Sankur and N. Memon. *Source Cell-Phone Identification*. IEEE Signal Processing and Communications Applications, pages 1–3, April 2006. (Cited on page 33.)

[Chan 2012] L.-H. Chan, N.-F. Law and W.-C. Siu. *A two dimensional camera identification method based on image sensor noise*. In Acoustics, Speech and Signal Processing (ICASSP), 2012 IEEE International Conference on, pages 1741–1744, March 2012. (Cited on page 31.)

[Chan 2013] Lit-Hung Chan, Ngai-Fong Law and Wan-Chi Siu. *A confidence map and pixel-based weighted correlation for PRNU-based camera iden-*

tification. Digital Investigation, vol. 10, no. 3, pages 215–225, 2013. (Cited on pages 51 and 56.)

[Chen 2007a] M. Chen, J. Fridrich, J. Lukáš and M. Goljan. *Imaging sensor noise as digital x-ray for revealing forgeries.* In Information Hiding, pages 342–358. Springer, 2007. (Cited on pages 22 and 27.)

[Chen 2007b] Mo Chen, Jessica Fridrich and Miroslav Goljan. *Digital imaging sensor identification (further study).* In Electronic Imaging 2007. International Society for Optics and Photonics, 2007. (Cited on pages 22 and 27.)

[Chen 2008] M. Chen, J. Fridrich, M. Goljan and J. Lukás. *Determining image origin and integrity using sensor noise.* Information Forensics and Security, IEEE Transactions on, vol. 3, no. 1, pages 74–90, 2008. (Cited on pages 22 and 27.)

[Cherry 2012] Simon R Cherry, James A Sorenson and Michael E Phelps. Physics in nuclear medicine. Elsevier Health Sciences, 2012. (Cited on page 11.)

[Chierchia 2010] Giovanni Chierchia, Sara Parrilli, Giovanni Poggi, Carlo Sansone and Luisa Verdoliva. *On the influence of denoising in PRNU based forgery detection.* In Proceedings of the 2nd ACM workshop on Multimedia in forensics, security and intelligence, pages 117–122. ACM, 2010. (Cited on page 31.)

[Choi 1998] Hyeokho Choi and Richard Baraniuk. *Analysis of wavelet-domain Wiener filters.* In Time-Frequency and Time-Scale Analysis, 1998. Proceedings of the IEEE-SP International Symposium on, pages 613–616. IEEE, 1998. (Cited on page 63.)

[Choi 2010] C.-H. Choi, M.-J. Lee and H.-K. Lee. *Scanner identification using spectral noise in the frequency domain.* In Image Processing (ICIP), 2010 17th IEEE International Conference on, pages 2121–2124, Sept 2010. (Cited on page 32.)

[Cierniak 2011] Robert Cierniak. X-ray computed tomography in biomedical engineering. Springer Science & Business Media, 2011. (Cited on page 14.)

[Costa 2012] H. B. Costa, R. F. Zampolo, D. M. Carmo, A. R. Castro and E. P. Santos. *On the practical aspects of applying the PRNU approach to device identification tasks.* International Conference on Multimedia Forensics, Surveillance and Security, September 2012. (Cited on page 24.)

[Cox 2002] Ingemar J Cox, Matthew L Miller, Jeffrey Adam Bloom and Chris Honsinger. Digital watermarking. Springer, 2002. (Cited on pages 24 and 29.)

[Del Cura 2012] Jose Luís Del Cura, Pedro Seguí and Carlos Nicolau. Learning ultrasound imaging. Springer Science & Business Media, 2012. (Cited on page 10.)

[Do 2005] Minh N Do and Martin Vetterli. *The contourlet transform: an efficient directional multiresolution image representation.* Image Processing, IEEE Transactions on, vol. 14, no. 12, pages 2091–2106, 2005. (Cited on page 35.)

[Doi 2006] Kunio Doi. *Diagnostic imaging over the last 50 years: research and development in medical imaging science and technology.* Physics in Medicine and Biology, vol. 51, no. 13, page R5, 2006. (Cited on page 2.)

[Duan 2014] Yuping Duan, Gouenou Coatrieux and Huazhong Shu. *Identification of digital radiography image source based on digital radiography pattern noise recognition.* In Image Processing (ICIP), 2014 IEEE International Conference on, pages 5372–5376. IEEE, 2014. (Cited on pages 34 and 92.)

[Duan 2015] Y. Duan, G. Coatrieux and H. Shu. *Computed tomography image source identification by discriminating CT-scanner image reconstruction process.* In Engineering in Medicine and Biology Society (EMBC), 2015 37th Annual International Conference of the IEEE, pages 5622–5625. IEEE, 2015. (Cited on pages 35 and 92.)

[Duan 2016] Yuping Duan, Dalel Bouslimi, Guanyu Yang, Huazhong Shu and Gouenou Coatrieux. *Computed Tomography Image Origin Identification based on Original Sensor Pattern Noise and 3D Image Reconstruction Algorithm Footprints.* 2016. (Cited on page 35.)

[Edelman 1993] Robert R Edelman and Steven Warach. *Magnetic resonance imaging.* New England Journal of Medicine, vol. 328, no. 10, pages 708–716, 1993. (Cited on page 8.)

[Farid 2008] Hany Farid. *Digital image forensics.* Scientific American, vol. 298, no. 6, pages 66–71, 2008. (Cited on page 22.)

[Farid 2009] Hany Farid. *Image forgery detection.* IEEE Signal processing magazine, vol. 26, no. 2, pages 16–25, 2009. (Cited on page 4.)

[Filler 2008] T. Filler, J. Fridrich and M. Goljan. *Using sensor pattern noise for camera model identification.* In Image Processing, 2008. ICIP 2008. 15th IEEE International Conference on, pages 1296–1299. IEEE, 2008. (Cited on page 28.)

[Fridrich 2009] Jessica Fridrich. *Digital image forensics.* IEEE Signal Processing Magazine, vol. 26, no. 2, pages 26–37, 2009. (Cited on page 4.)

[Geradts 2002] Zeno J Geradts, Jurrien Bijhold, Martijn Kieft, Kenji Kurosawa*et al.* *Digital camera identification.* Journal of Forensic Identification, vol. 52, no. 5, page 621, 2002. (Cited on page 22.)

[Goljan 2008a] Miroslav Goljan. *Digital camera identification from images–estimating false acceptance probability.* In International Workshop on Digital Watermarking, pages 454–468. Springer, 2008. (Cited on page 85.)

[Goljan 2008b] Miroslav Goljan and Jessica Fridrich. *Camera Identification from Scaled and Cropped Images.* In Edward J. Delp and Ping Wah Wong, editeurs, SPIE Conference on Security, Forensics, Steganography, and Watermarking of Multimedia Contents, volume 6819, 2008. (Cited on pages 24 and 28.)

[Goljan 2009] M. Goljan, J. Fridrich and T. Filler. *Large scale test of sensor fingerprint camera identification.* In IS&T/SPIE Electronic Imaging. International Society for Optics and Photonics, 2009. (Cited on pages 29, 42 and 85.)

[Goljan 2011] Miroslav Goljan, Jessica Fridrich and Mo Chen. *Defending against fingerprint-copy attack in sensor-based camera identification.* IEEE Transactions on Information Forensics and Security, vol. 6, no. 1, pages 227–236, 2011. (Cited on page 98.)

[Graham 2005] RNJ Graham, RW Perriss and AF Scarsbrook. *DICOM demystified: a review of digital file formats and their use in radiological practice.* Clinical Radiology, vol. 60, no. 11, pages 1133–1140, 2005. (Cited on page 2.)

[Hounsfield 1980] Godfrey N Hounsfield. *Computed medical imaging.* Journal of computer assisted tomography, vol. 4, no. 5, pages 665–674, 1980. (Cited on pages 17 and 83.)

[Hsieh 2004] J Hsieh, E Chao, J Thibault, B Grekowicz, A Horst, S McOlash and TJ Myers. *A novel reconstruction algorithm to extend the CT scan field-of-view.* Medical Physics, vol. 31, no. 9, pages 2385–2391, 2004. (Cited on page 14.)

[Hsieh 2006] Jiang Hsieh, John Londt, Melissa Vass, Jay Li, Xiangyang Tang and Darin Okerlund. *Step-and-shoot data acquisition and reconstruction for cardiac x-ray computed tomography.* Medical Physics, vol. 33, no. 11, pages 4236–4248, 2006. (Cited on page 14.)

[Hsieh 2009] Jiang Hsieh. *Computed tomography: principles, design, artifacts, and recent advances.* SPIE Bellingham, WA, 2009. (Cited on page 11.)

[Hsieh 2013] Jiang Hsieh, Brian Nett, Zhou Yu, Ken Sauer, Jean-Baptiste Thibault and Charles A Bouman. *Recent advances in CT image reconstruction.* Current Radiology Reports, vol. 1, no. 1, pages 39–51, 2013. (Cited on page 14.)

[Hu 1999] Hui Hu. *Multi-slice helical CT: scan and reconstruction.* Medical physics, vol. 26, no. 1, pages 5–18, 1999. (Cited on page 69.)

[Huang 2012] H. Huang, G. Coatrieux, H. Shu, L. Luo and C. Roux. *Blind Integrity Verification of Medical Images.* IEEE Transactions on Information Technology in Biomedicine, vol. 16, no. 6, pages 1122–1126, 2012. (Cited on page 33.)

[Jacob 2004] Nevine Jacob and Aline Martin. *Image denoising in the wavelet domain using wiener filtering.* Unpublished course project, University of Wisconsin, Madison, Wisconsin, USA, 2004. (Cited on page 63.)

[Jenkins 2009] Neil Jenkins. *Digital camera identification.* 2009. (Cited on page 22.)

[Jerhotová 2011] Eva Jerhotová, Aleš Procházka and Jan Švihlík. Biomedical image volumes denoising via the wavelet transform. INTECH Open Access Publisher, 2011. (Cited on page 63.)

[Jones 2013] David Wyn Jones, Peter Hogg and Euclid Seeram. Practical SPECT/CT in nuclear medicine. Springer, 2013. (Cited on page 15.)

[Kagadis 2011] George C Kagadis and Steve G Langer. Informatics in medical imaging. CRC Press, 2011. (Cited on page 16.)

[Kang 2012] X. Kang, Y. Li, Z. Qu and J. Huang. *Enhancing Source Camera Identification Performance With a Camera Reference Phase Sensor Pattern Noise.* Information Forensics and Security, IEEE Transactions on, vol. 7, no. 2, pages 393–402, April 2012. (Cited on page 29.)

[Kazubek 2003] Marian Kazubek. *Wavelet domain image denoising by thresholding and Wiener filtering.* IEEE Signal Processing Letters, vol. 10, no. 11, pages 324–326, 2003. (Cited on page 63.)

[Ketcham 2001] Richard A Ketcham and William D Carlson. *Acquisition, optimization and interpretation of X-ray computed tomographic imagery: applications to the geosciences.* Computers & Geosciences, vol. 27, no. 4, pages 381–400, 2001. (Cited on page 13.)

[Khanna 2007] N. Khanna, A. K. Mikkilineni, G. T.-C. Chiu, J. P. Allebach and E. J. Delp. *Scanner Identification Using Sensor Pattern Noise.* In Edward J. Delp and Ping Wah Wong, editeurs, SPIE Conference on Security, Steganography, and Watermarking of Multimedia Contents, volume 6505, 2007. (Cited on page 32.)

[Kharboutly 2014] Anas Kharboutly, William Puech, Gérard Subsol and Denis Hoa. *CT-Scanner identification based on sensor noise analysis.* In Visual Information Processing (EUVIP), 2014 5th European Workshop on, pages 1–5. IEEE, 2014. (Cited on page 5.)

[Kharboutly 2015a] Anas Kharboutly, William Puech, Gérard Subsol and Denis Hoa. *Advanced sensor noise analysis for CT-scanner identification from its 3D images.* In Image Processing Theory, Tools and Applications (IPTA), 2015 International Conference on, pages 325–330. IEEE, 2015. (Cited on page 5.)

[Kharboutly 2015b] Anas Kharboutly, William Puech, Gérard Subsol and Denis Hoa. *Improving sensor noise analysis for CT-Scanner identification.* In Signal Processing Conference (EUSIPCO), 2015 23rd European, pages 2411–2415. IEEE, 2015. (Cited on page 5.)

[Kharrazi 2004] M. Kharrazi, H. T. Sencar and N. Memon. *Blind source camera identification.* In Image Processing, 2004. ICIP '04. 2004 International Conference on, volume 1, pages 709–712 Vol. 1, 2004. (Cited on page 33.)

[Kuperman 2000] Vadim Kuperman. Magnetic resonance imaging: physical principles and applications. Academic Press, 2000. (Cited on page 9.)

[Lehmann 1999] Thomas Martin Lehmann, Claudia Gonner and Klaus Spitzer. *Survey: Interpolation methods in medical image processing.* IEEE transactions on medical imaging, vol. 18, no. 11, pages 1049–1075, 1999. (Cited on page 97.)

[Leondes 2005] Cornelius T Leondes. Medical imaging systems technology: Methods in cardiovascular and brain systems, volume 5. World Scientific, 2005. (Cited on page 8.)

[Lewis 1992] Adrian S Lewis and G Knowles. *Image compression using the 2-D wavelet transform*. IEEE Transactions on image Processing, vol. 1, no. 2, pages 244–250, 1992. (Cited on page 97.)

[Li 2010] C. T. Li. *Source Camera Identification Using Enhanced Sensor Pattern Noise*. Trans. Info. For. Sec., vol. 5, no. 2, pages 280–287, 2010. (Cited on page 30.)

[Li 2012] Shutao Li, Leyuan Fang and Haitao Yin. *An efficient dictionary learning algorithm and its application to 3-D medical image denoising*. IEEE Transactions on Biomedical Engineering, vol. 59, no. 2, pages 417–427, 2012. (Cited on page 97.)

[Lisle 2012] David A Lisle. Imaging for students. Fourth Edition. CRC Press, 2012. (Cited on page 11.)

[Liu 2009] Shaohui Liu, Lin Ma, Hongxun Yao and Debin Zhao. *Universal steganalysis based on statistical models using reorganization of block-based DCT coefficients*. In Information Assurance and Security, 2009. IAS'09. Fifth International Conference on, volume 1, pages 778–781. IEEE, 2009. (Cited on page 33.)

[Liu 2010] Bei-Bei Liu, Yongjian Hu and Heung-Kyu Lee. *Source camera identification from significant noise residual regions*. In 2010 IEEE International Conference on Image Processing, pages 1749–1752. IEEE, 2010. (Cited on page 4.)

[Lukas 2006] J. Lukas, J. Fridrich and M. Goljan. *Digital camera identification from sensor pattern noise*. IEEE Transactions on Information Forensics and Security, vol. 1, no. 2, pages 205–214, 2006. (Cited on pages 22, 23, 24, 28, 35, 36, 37, 41, 42 and 63.)

[Mahdian 2010] Babak Mahdian and Stanislav Saic. *A bibliography on blind methods for identifying image forgery.* Signal Processing: Image Communication, vol. 25, no. 6, pages 389–399, 2010. (Cited on page 22.)

[McAuliffe 2001] Matthew J McAuliffe, Francois M Lalonde, Delia McGarry, William Gandler, Karl Csaky and Benes L Trus. *Medical image processing, analysis and visualization in clinical research.* In Computer-Based Medical Systems, 2001. CBMS 2001. Proceedings. 14th IEEE Symposium on, pages 381–386. IEEE, 2001. (Cited on page 2.)

[Mettler Jr 2011] Fred A Mettler Jr and Milton J Guiberteau. Essentials of nuclear medicine imaging. Elsevier Health Sciences, 2011. (Cited on page 11.)

[Mihcak 1999] M Kivanc Mihcak, Igor Kozintsev and Kannan Ramchandran. *Spatially adaptive statistical modeling of wavelet image coefficients and its application to denoising.* In Acoustics, Speech, and Signal Processing, 1999. Proceedings., 1999 IEEE International Conference on, volume 6, pages 3253–3256. IEEE, 1999. (Cited on pages 25 and 63.)

[Mohammadnejad 2011] S. Mohammadnejad, S. Roshani and M. N. Sarvi. *Fixed pattern noise reduction method in CCD sensors for LEO satellite applications.* In Telecommunications (ConTEL), Proceedings of the 2011 11th International Conference on, pages 441–446. IEEE, 2011. (Cited on page 23.)

[Nitzberg 1993] Mark Nitzberg, David Mumford and Takahiro Shiota. Filtering, segmentation and depth. 1993. (Cited on page 54.)

[Pan 2010] Wei Pan, Gouenou Coatrieux, Nora Cuppens-Boulahia, Frederic Cuppens and Christian Roux. *Medical image integrity control combining digital signature and lossless watermarking.* In Data privacy

management and autonomous spontaneous security, pages 153–162. Springer, 2010. (Cited on page 3.)

[Pianykh 2012] Oleg S Pianykh. *What Is DICOM?* In Digital Imaging and Communications in Medicine (DICOM), pages 3–5. Springer, 2012. (Cited on page 2.)

[Piva 2013] A. Piva. *An overview on image forensics.* ISRN Signal Processing, vol. 2013, 2013. (Cited on pages xiii, 22 and 26.)

[Redi 2011] J. Redi, W. Taktak and J. L. Dugelay. *Digital image forensics: a booklet for beginners.* Multimedia Tools and Applications, vol. 51, no. 1, pages 133–162, 2011. (Cited on page 22.)

[Rosenfeld 2009] Kurt Rosenfeld and Husrev T Sencar. *A study of the robustness of prnu-based camera identification.* In IS&T/SPIE Electronic Imaging, pages 72540M–72540M. International Society for Optics and Photonics, 2009. (Cited on page 98.)

[Satheesh 2011] S Satheesh and KVSVR Prasad. *Medical image denoising using adaptive threshold based on contourlet transform.* arXiv preprint arXiv:1103.4907, 2011. (Cited on pages 35 and 97.)

[Seeram 2015] Euclid Seeram. Computed tomography: physical principles, clinical applications, and quality control. Elsevier Health Sciences, 2015. (Cited on pages xiii, 2, 12, 13 and 15.)

[Sencar 2013] H. T. Sencar and N. Memon. Digital image forensics: There is more to a picture than meets the eye. Springer, 2013. (Cited on page 22.)

[Sezgin 2004] Mehmet Sezgin*et al. Survey over image thresholding techniques and quantitative performance evaluation.* Journal of Electronic imaging, vol. 13, no. 1, pages 146–168, 2004. (Cited on page 82.)

[Shi 2005] Yun Q Shi, Guorong Xuan, Dekun Zou, Jianjiong Gao, Chengyun Yang, Zhenping Zhang, Peiqi Chai, Wen Chen and Chunhua Chen. *Image steganalysis based on moments of characteristic functions using wavelet decomposition, prediction-error image, and neural network.* In ICME, volume 2005, pages 269–272, 2005. (Cited on page 33.)

[Shi 2014] C. Shi, N.-F. Law, H.-F. Leung and W.-C. Siu. *Weighting optimization with neural network for photo-response-non-uniformity-based source camera identification.* In Asia-Pacific Signal and Information Processing Association, 2014 Annual Summit and Conference (APSIPA), pages 1–7, Dec 2014. (Cited on page 30.)

[Solomon 2012] J. B. Solomon, O. Christianson and E. Samei. *Quantitative comparison of noise texture across CT scanners from different manufacturers.* Medical Physics, vol. 39, no. 10, pages 6048–55, October 2012. (Cited on page 33.)

[Strela 2001] Vasily Strela. *Denoising via block Wiener filtering in wavelet domain.* In European Congress of Mathematics, pages 619–625. Springer, 2001. (Cited on page 98.)

[Sutton 1987] David Sutton. *A textbook of radiology and imaging.* 1987. (Cited on page 8.)

[Taubman 2012] David Taubman and Michael Marcellin. Jpeg2000 image compression fundamentals, standards and practice: Image compression fundamentals, standards and practice, volume 642. Springer Science & Business Media, 2012. (Cited on page 97.)

[Toennies 2012] Klaus D. Toennies. Guide to medical image analysis - methods and algorithms. Advances in Computer Vision and Pattern Recognition. Springer, 2012. (Cited on page 18.)

[Von Ramm 1990] Olaf T Von Ramm and Stephen W Smith. *Real-time volumetric ultrasound imaging system.* In Medical Imaging'90, Newport Beach, 4-9 Feb 90, pages 15–22. International Society for Optics and Photonics, 1990. (Cited on page 9.)

[Wang 2006] Ying Wang and Pierre Moulin. *Statistical modelling and steganalysis of DFT-based image steganography.* In Electronic Imaging 2006. International Society for Optics and Photonics, 2006. (Cited on page 33.)

[Wolbarst 2013] Anthony B Wolbarst, Patrizio Capasso and Andrew R Wyant. Medical imaging: Essentials for physicians. John Wiley & Sons, 2013. (Cited on page 8.)

[Yerushalmy 2011] Ido Yerushalmy and Hagit Hel-Or. *Digital image forgery detection based on lens and sensor aberration.* International Journal of Computer Vision, vol. 92, no. 1, pages 71–91, 2011. (Cited on page 4.)

[Zhang 2012] Yang Zhang, Peng Xia, Junzhou Luo, Zhen Ling, Benyuan Liu and Xinwen Fu. *Fingerprint attack against touch-enabled devices.* In Proceedings of the second ACM workshop on Security and privacy in smartphones and mobile devices, pages 57–68. ACM, 2012. (Cited on page 98.)

[Zhong 2004] Junmei Zhong, Ruola Ning and David Conover. *Image denoising based on multiscale singularity detection for cone beam CT breast imaging.* IEEE transactions on medical imaging, vol. 23, no. 6, pages 696–703, 2004. (Cited on page 97.)

Identification of the Acquisition System in Medical Images by Noise Analysis

Abstract: Medical image processing aims to help the doctors to improve the diagnosis process. Computed Tomography (CT) Scanner is an imaging medical device used to create cross-sectional 3D images of any part of the human body. Today, it is very important to secure medical images during their transmission, storage, visualization and sharing between several doctors. For example, in image forensics, a current problem consists of being able to identify an acquisition system from only digital images. In this thesis, we present one of the first analysis of CT-Scanner identification problem. We based on the camera identification methods to propose a solution for such kind of problem. It is based on extracting a sensor noise fingerprint of the CT-Scanner device. The objective then is to detect its presence in any new tested image. To extract the noise, we used a wavelet-based Wiener denoising filter. Then, we depend on the properties of medical images to propose advanced solutions for CT-Scanner identification. These solutions are based on new conceptions in the medical device fingerprint that are the three dimension fingerprint and the three layers one. To validate our work, we applied our experiments on multiple real data images of multiple CT-Scanner devices. Finally, our methods that are robust, give high identification accuracy. We were able to identify the acquisition CT-Scanner device and the acquisition axis.

Keywords: Medical image forensics, device identification, sensor noise, denoise filtering, device fingerprint.